Tutorials and Reviews

International Journal of Bifurcation and Chaos, Vol. 12, No. 11 (2002) 2307–2332

DIFFUSIVE INSTABILITIES AND CHEMICAL REACTIONS

P. BORCKMANS, G. DEWEL and A. DE WIT
Center for Nonlinear Phenomena and Complex Systems,
CP 231, Université Libre de Bruxelles,
1050 Brussels, Belgium

E. DULOS, J. BOISSONADE, F. GAUFFRE and P. DE KEPPER
Centre de Recherche Paul Pascal/CNRS,
Université Bordeaux I,
Avenue A. Schweitzer, 33600 Pessac, France

Received January 4, 2002; Revised February 1, 2002

Diffusive instabilities provide the engine for an ever increasing number of dissipative structures. In this class autocatalytic chemical systems are prone to generate temporal and spatial self-organization phenomena. The development of open spatial reactors and the subsequent discovery in 1989 of the stationary reaction–diffusion patterns predicted by Turing [1952] have triggered a large amount of research. This review aims at a comparison between theoretical predictions and experimental results obtained with various type of reactors in use. The differences arising from the use of reactions exhibiting either bistability of homogeneous steady states or a single one in a CSTR are emphasized.

Keywords: Symmetry breaking; gel reactor; spatial bistability.

1. Introduction

Pattern formation far from thermodynamic equilibrium, i.e. the generation of *dissipative structures* [Glansdorff & Prigogine, 1971; Nicolis & Prigogine, 1977], now encompasses an impressive corpus of data in an ever increasing diversity of fields. These structures, sustained by a permanent throughput of mass or energy, are characterized by the temporal and/or spatial modulation of their properties (temperature, concentrations, velocity, stress, electric fields, ...). Our understanding of spatial patterns has now progressed far beyond the properties of the paradigmatic Bénard convection cell structures [Cross & Hohenberg, 1993]. Among the scores of such self-organizing systems, a specific class of problems is generated by *diffusive instabilities* as proposed by Turing [1952] in chemical reaction–diffusion systems. This spontaneous instability of an homogeneous mixture of chemically reacting species, when some parameter threshold is crossed, leads to stationary, space-periodic patterns of the concentrations of reactants. To support such symmetry breaking instability, the chemical kinetics has to involve some type of positive feedback loop controlled by an *activator species* that reinforces its own changes, the latter being counterbalanced by an *inhibitory process*. Spatial structures can form when the inhibitory effects are transported by diffusion over a larger space range than that of the activatory mechanism. This allows for the local growth of the activator while the lateral inhibition prevents the spreading of the activation centre. When such process competition

repeats itself, it finally leads to a stationary periodic pattern, the wavelength of which is solely a function of the values of the diffusion coefficients and of the kinetic parameters, and not of some geometrical length characteristic of the experimental device being used. Although our discussion will focus on such chemical systems, diffusive instabilities remain pertinent to the formation of structures in many other fields such as electron-hole plasmas in semiconductors [Kerner & Osipov, 1994], gas discharge devices [Willebrand *et al.*, 1992; Radehaus, 1992], semiconductor structures (*p-n* junctions, *p-i-n* diodes) [Schöll, 1987; Niedernostheide, 1992], heterogeneous catalysis [Falta *et al.*, 1990], electrochemistry [Li *et al.*, 2001], nonlinear optics [Lugiato *et al.*, 1998; Arecchi *et al.*, 1999], materials irradiated with energetic particles or light [Krishan, 1980; Emelyanov, 1992; Walgraef, 1996]. The description of all these systems can indeed formally be cast in the common language of reaction–diffusion systems governed by the following set of equations:

$$\frac{\partial \mathbf{c}(\mathbf{r}, t)}{\partial t} = \mathbf{f}(\mathbf{c}, b) + D\nabla^2\mathbf{c}(\mathbf{r}, t)\,, \qquad (1)$$

where $\mathbf{c}(\mathbf{r}, t)$ is the local concentration vector, $\mathbf{f}(\mathbf{c}, b)$ is a vector function representing the reaction kinetics, b stands for a set of control parameters and D is the matrix of constant diffusive transport coefficients. Appropriate initial and boundary conditions, in relation with the experiments, should also be added to complete the mathematical formulation. In some situations, Eq. (1) should be extended to include integral conditions on the variables or advective terms if flow is present (see conclusions). A *Turing pattern* forming instability occurs when perturbations of given wave numbers applied to the homogeneous steady state (HSS) of reference are able to grow spontaneously. The threshold conditions are usually obtained through a linear stability analysis of this HSS which also determines the order of magnitude of the characteristic wave number of the emerging structure. Theoretical work relies heavily on the use of nonlinear kinetic models for $\mathbf{f}(\mathbf{c}, b)$ with a limited number of chemical species, typically two or three. These models stand as a compromise between a minimum of chemical realism and mathematical tractability as the experimental schemes usually involve a large amount of species, often not yet unequivocally determined. Pattern selection, using the paraphernalia of bifurcation theoretical methods [Manneville, 1990; Cross & Hohenberg, 1993; Nicolis, 1995], leads to the construction of bifurcation diagrams through the derivation and analysis of so-called *amplitude equations* for the active spatial (Fourier) modes. These modes are responsible for the loss of stability of the reference HSS state by growing exponentially. They do so by drawing on the imposed driving force and end up competing nonlinearly to create new stable modulated solutions. The number of such modes increases as one moves further beyond the instability point. In systems the size of which is large with respect to the characteristic wavelength, a large multiplicity of solutions becomes possible. The outcome of analytical work allows to determine which structures with given symmetry are stable for definite conditions (*bifurcation diagram*). It also helps to organize the results obtained by straightforward numerical integration of the reaction–diffusion equations. Both informations may finally be used to interpret the experimental results.

The experimental work takes place in so-called *open spatial reactors*, described further on, that are specifically designed to control the reaction and the structures that eventually develop at a fixed distance from equilibrium and allow to probe the true asymptotic states of the reaction–diffusion systems. To this effect, they are constructed to avoid all perturbations induced by the hydrodynamic flows associated with the constant supply of fresh reactants. They must also enable the necessary diffusion differential between activator and inhibitor species to permit Turing and other spatial instabilities to occur. The systems we discuss are also prone to exhibit various homogeneous bifurcations, either to time oscillations (Hopf) or to multiplicity of HSS (saddle-node, pitchfork, etc) as their nonlinearities stem from the local kinetics (unlike hydrodynamics where they usually originate from convective or advective contributions). Therefore, when diffusive effects are also included, it is not at all surprising to observe other bifurcations competing with the Turing instability, thereby giving rise to a rich variety of behaviors. Although a huge amount of theoretical and numerical work, among which many contributions by Manuel Velarde [Velarde, 1981], Turing structures were actually first observed late in 1989 by some of us [Castets *et al.*, 1990]. The present paper outlines some experimental and theoretical development of the research that resulted from this discovery by making a distinction between the cases where the system exhibits single or multiple HSS.

2. Monostable Systems

The analytical work to determine the bifurcation diagram near a Turing-type instability (or any space-symmetry breaking instability) has by now become a standard procedure. Here, we sketch the principles of this derivation referring the reader to typical monographs for technical details [Manneville, 1990; Cross & Hohenberg, 1993; Nicolis, 1995]. To analyze the system behavior in the vicinity of the control parameter threshold, b_T, one proceeds by expanding the difference of the concentration field $\mathbf{c}(\mathbf{r}, t)$ from its reference state $\mathbf{c}_*$ as an asymptotic series:

$$\mathbf{c}(\mathbf{r}, t) - \mathbf{c}_* = \varepsilon \mathbf{c}_1 + \varepsilon^2 \mathbf{c}_2 + \varepsilon^3 \mathbf{c}_3 + \cdots , \qquad (2)$$

where the small expansion parameter ε is related to the distance μ from threshold by

$$\mu \sim b - b_T = \varepsilon b_1 + \varepsilon^2 b_2 + \varepsilon^3 b_3 + \cdots \qquad (3)$$

The first order contribution $\mathbf{c}_1$ is a linear combination of the active modes given by suitable eigenfunctions of the Laplacian operator. Now, it is known from linear stability analysis, that for large aspect ratio systems, one has to take into account two kinds of degeneracies in the determination of the active modes. The rotational degeneracy may be tackled first, ignoring in this step the effects arising from the presence of sidebands. At the leading order of approximation one writes:

$$\mathbf{c}_1 = \mathbf{e}_T \sum_{i=1}^{M} [A_i(\tau) \exp(i\mathbf{q}_i \cdot \mathbf{r}) + cc] , \qquad (4)$$

where $\mathbf{e}_T$ is the critical eigenvector of the linear evolution operator. The complex amplitudes A_i take the translational invariance of the infinite system into account (cc holds for complex conjugate). The set of M pairs of wavevectors $\mathbf{q}_i$, $-\mathbf{q}_i$ characterizing the active modes are chosen on the critical circle (2D) or sphere (3D), $|\mathbf{q}| = q_c$ in q-space. Because concentrations are real, the active modes involve pairs of opposite wavevectors. Each set defines a possible pattern and the amplitude equations we have set out to obtain will determine which pattern is favored by the nonlinear interactions. The amplitudes A_i depend on the natural slow time scale of the critical modes; this time scale is proportional to $1/\mu(\tau = \mu t)$. The expansions (2)–(4) are inserted in the nonlinear reaction–diffusion equations. Equating the successive powers of ε leads to a hierarchy of linear inhomogeneous equations that are solved recursively. The solvability conditions of these inhomogeneous equations (Fredholm alternative theorem) then lead to a set of ODEs, the amplitude equations for the active modes that are of the form

$$\frac{dA_i}{dt} = \mu A_i + G_i(A_j) , \qquad (5)$$

where $G_i(A_j)$ are nonlinear polynomials in the active amplitudes. These equations are universal in character and the information concerning a particular system is solely contained in the structure of the polynomials and their coefficients. The second degeneracy is related to the existence of the sideband modes that also interact nonlinearly with the critical modes. Indeed, as one moves beyond b_T, a continuous band of modes with wavenumbers bracketing q_c becomes active. Taking into account the beating of all these modes allows the derivation of so-called envelope amplitude equations (PDE's), that will not be considered here but are necessary to describe the modulations of the amplitudes over lengths large compared to q_c^{-1} as well as defects and spatiotemporal chaos [Newell *et al.*, 1993].

Near b_T when the saturation of the instability occurs at the lowest order and for systems exhibiting a single HSS (monostable situation) the complex amplitude equations, for a 2D system, have the following general structure:

$$\frac{dA_i}{dt} = \frac{b - b_T}{b_T} A_i + v \sum_{j}^{M} \sum_{k}^{M} A_j^* A_k^* \delta(\mathbf{q}_i + \mathbf{q}_j + \mathbf{q}_k) - g_D |A_i|^2 A_i - \sum_{j \neq i}^{M} g_{ND} |A_j|^2 A_i \qquad (6)$$

for $i = 1, \ldots, M$. This equation mainly supports solutions such as stripes ($M = 1$), squares ($M = 2$) and patterns of triangular symmetry ($M = 3$) or even quasiperiodic structures ($M > 3$). Because in chemical systems $g_{ND} > g_D$, squares and quasiperiodic patterns are never stable. If $A_i = R_i e^{i\phi_i}$, the phase ϕ_i of the stripes (concentration modulations along one direction) is free as it solely determines their position with respect to an arbitrary set of reference axis. For $M = 3$, three phase factors come into play; as two are sufficient to set the position of the planform, the third one or the sum Φ of the three phases, must be determined dynamically hence the "resonant" qualifier applied to the resulting patterns. It turns out that, depending on the sign of the quadratic coupling v, one has either

h_0 hexagons ($v > 0$ and $\Phi = 0$) when the maxima of concentration form a triangular lattice or h_π hexagons ($v < 0$ and $\Phi = \pi$) when the maxima form a honeycomb lattice.

In the frame of this nonlinear theory, the hexagons are the first to appear subcritically. Increasing the value of the bifurcation parameter b, the hexagons become unstable with respect to the stripes, the branch of which has emerged supercritically. Reversing the variation of b allows one to recover the hexagonal structure but by undergoing a hysteresis loop. This is the "universal" hex-stripes competition scenario that comes up in many different fields of study [Haken & Olbrich, 1978; Pismen, 1980; Walgraef *et al.*, 1980; Walgraef *et al.*, 1982]. In the bistable stripes-hexagons region, metastability determines which structure is favored depending on the precise experimental set-up. When metastability is taken into account, the hysteresis loop may altogether not be seen [Borckmans *et al.*, 1992]. Modifications of this scenario in the vicinity of the primary bifurcation point b_T include the situation where the cubic coupling g_D is such that the branch of stripes also appears subcritically. This can actually occur for the Lengyel–Epstein model describing the CDIMA reaction to be discussed shortly. Higher order terms must then be retained in the amplitude equation. The structure of the amplitude equations is also modified if the Turing bifurcation interacts with other homogeneous bifurcations, a possibility which was alluded to previously. The result is the appearance of new mixed mode solutions that were studied in detail for the Turing–Hopf interaction [Kidachi, 1980; De Wit *et al.*, 1993, 1996] and which will be commented on in relation to the experiments. The organizing center of the bifurcation calculation is then the so-called Turing–Hopf (codimension-two) point where both bifurcations coalesce. The interaction of Turing instabilities with other homogeneous bifurcations in relation to bistability of HSS will be discussed in Sec. 3. In 3D systems, the following standard sequence may be obtained: body centered cubic, hexagonal prisms, lamellae [Walgraef *et al.*, 1980; De Wit *et al.*, 1992, 1997; Pismen, 1994; Callahan & Knobloch, 1996, 1999].

The experimental studies of chemical patterns in solution chemistry are carried out in "reactors" the design of which has considerably progressed with time. In closed reactors (batch), only transient spatial organizations can be observed as the system eventually relaxes to equilibrium. In order to maintain stable nonhomogeneous states and characterize the bifurcations between them, the system must be kept at a controlled distance from equilibrium, a requirement satisfied by making use of open spatial reactors. Many geometries of such reactors have been developed and, in the following, we shall focus on the most popular designs. The core of these reactors is very often made of a disc of soft hydrogel (polyacrylamide, agarose, polyvinylalcohol) fed by diffusion from only one [Fig. 1(b)] or the two [Fig. 1(a)] circular faces with chemicals contained in stirred tanks (CST) the contents of which are continuously renewed by pumps. The gel is used to prevent any fluid motion, so that the only processes at work within it are reactions and diffusion.

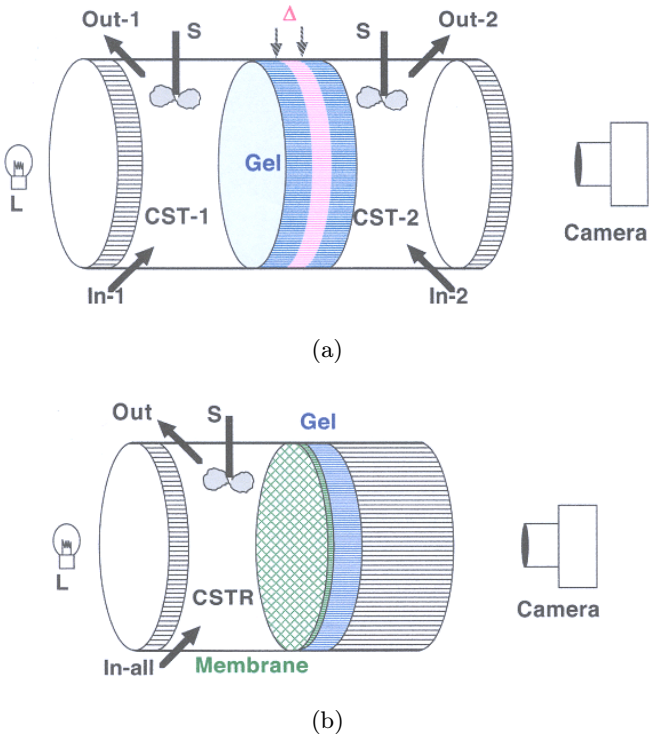

Fig. 1. Schematic representation of open spatial reactors: (a) disc shaped two-side-fed reactor (TSFR); CST-1 and CST-2 are continuous stirred tanks fed with complementary subsets of reactants. The typical gel-disc thickness is 3 mm. Δ: width of the stratum over which chemical patterns of characteristic wavelength λ develop. (b) disc shaped one-side-fed reactor (OSFR); CSTR (continuous stirred tank reactor), membrane (mineral disc, pore size 0,02 μm). Gel (2% agarose), in and out (input and output ports of chemicals), L (light source), CCD camera (black and white or color).

2.1. *Two-side-fed reactors (TSFR)*

The first experimental observations of Turing patterns [Castets *et al.*, 1990; Ouyang & Swinney, 1991]

were obtained in two-side-fed reactors (TSFR) [Fig. 1(a)] operated with the CIMA (chlorite-iodide-malonic acid) reaction [De Kepper *et al.*, 1982]. In this and related reactions, iodide (I^-) and chlorite (ClO_2^-) respectively play the role of the main activator and inhibitor species [Lengyel & Epstein, 1990; De Kepper *et al.*, 1990]. A basic solution of chlorite was fed on one side of the gel while an acidic solution of iodide and malonic acid (MA) was fed on the other side. In the experiments illustrated in this paper, the core of the reactor is made of agarose gel loaded with polyvinylalcohol (PVA), a macromolecule that plays two roles: (i) that of color indicator for the reaction. It forms a reddish-purple complex in the presence of iodine and iodide species and it is colorless in the absence of iodide. (ii) Consequently, this macromolecule of reduced mobility, by forming a fast reversible complex with these species, leads to an effective reduced diffusivity of the activator [Lengyel & Epstein, 1992; Pearson & Bruno, 1992], a necessary condition for Turing pattern formation. In the TSFR, the feed mode naturally induces ramps of chemical concentrations between the two opposite feed faces. Patterns only develop in a stratum of thickness Δ confined between these faces, where threshold conditions are overshot. Observations are made across the circular faces of the gel and patterns are seen to spread over the whole view plane. If the pattern stratum is sufficiently confined ($\Delta \leq \lambda$), it is said that the pattern develops in a monolayer [Dufiet & Boissonade, 1996]. If this stratum is less confined ($\Delta \geq \lambda$), patterns can develop in two or more layers [Ouyang *et al.*, 1992; Dulos *et al.*, 1996; Rudovics *et al.*, 1996].

The phase diagram of Fig. 2, established in the plane ($[I^-]_0$, $[MA]_0$)[1] [Rudovics *et al.*, 1996], shows three main regions. In region I, only the uniform state is stable (no symmetry breaking pattern). Region II exhibits stationary Turing patterns (the subregions correspond to various planforms). Region III gathers different time-dependent structures. These regions are separated by two lines, TT'P and HPH', which respectively correspond to the Turing and Hopf bifurcation lines. No hysteresis was unambiguously observed as a function of the malonic acid feed concentration, within our experimental accuracy.

Below a critical value of the iodide feed concentration, no symmetry breaking pattern and no time dependent structure are observed, only a uniform state (HSS) is detected over the whole range of malonic acid concentration tested. At this critical value, the Turing and Hopf lines suddenly curve and collide at the point P. This is a Turing–Hopf codimension-2 point around which the two instabilities develop from the uniform stationary state.

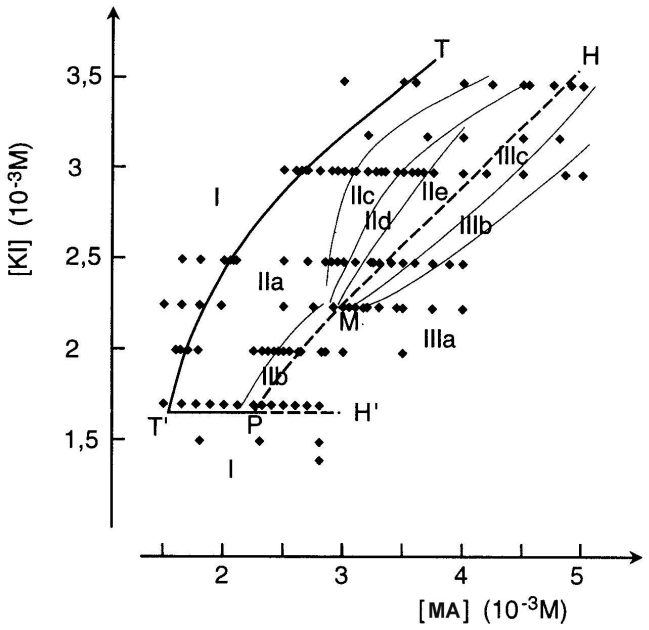

Fig. 2. Phase diagram obtained with the CIMA reaction operated in a two-side-fed reactor (TSFR). Section in the ($[MA]_0$, $[I^-]_0$)-plane; MA = malonic acid. For more details see reference [Rudovics *et al.*, 1996].

Let us now successively review the three regions beginning by the stationary patterns. As predicted by theory of two-dimensional systems, the first stable pattern mode observed (subregion IIa) is an hexagonal array of spots [Fig. 3(a)]. This region is followed (subregion IIb), at low $[I^-]_0$ by a domain of stripe (or band) pattern [Fig. 3(b)]. The typical wavelength of all these patterns is 0.2 mm. Note that close to point P, the band pattern seems to develop at onset; this would infer that the quadratic term of the Turing normal form drops to zero in this region of the phase diagram. At higher iodide feed concentration, more unusual planforms are observed: they are the symmetric triangles [Fig. 3(c)] of region IIc and the mixed hexagon and stripe modes ("hexa-bands") [Fig. 3(d)] of subregion IId. In addition, an intricate mixture of more or less symmetric triangles, hexa-bands and poorly contrasted stripes is found in subregion IIe.

[1] $[C_i]_0$ stands for the concentration of species C_i in the feed flux of the tanks, prior to any reaction.

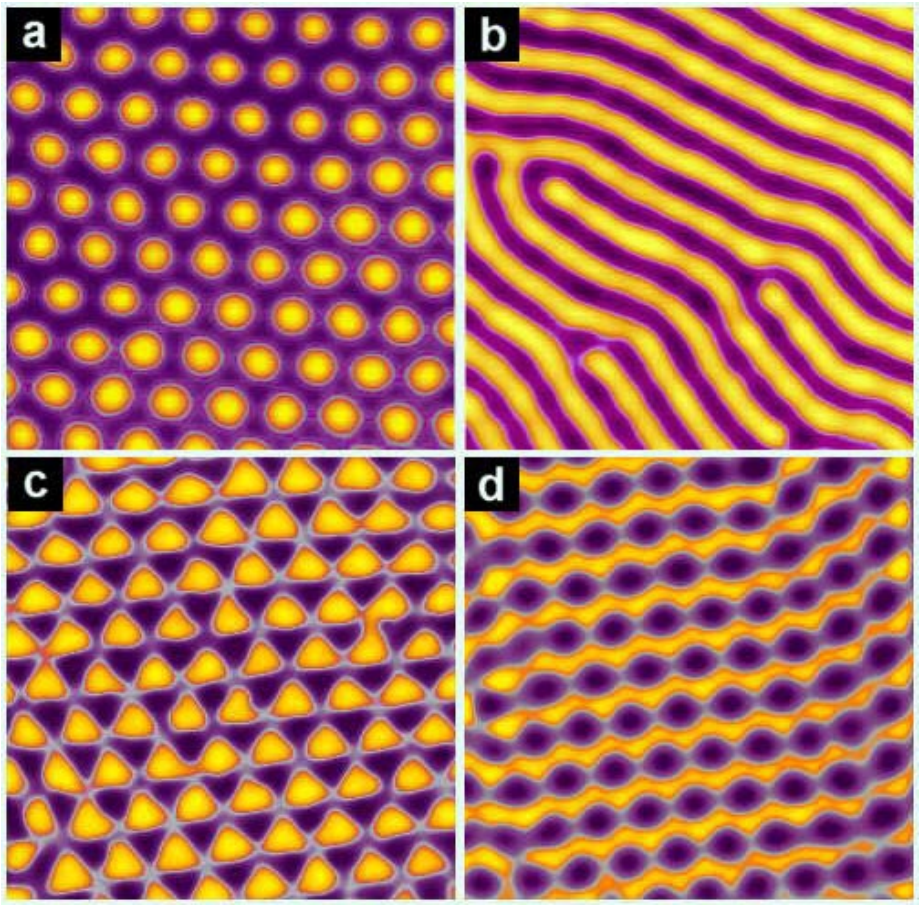

Fig. 3. Stationary pattern planforms corresponding to different subregions II of Fig. 2. Standard patterns: (a) hexagonal array of "clear" spots, (b) array of parallel stripes (bands). Nonstandard patterns: (c) array of symmetric triangles, (d) array of "dark" hexa-bands. All patterns are at the same scale: view size 1.7×1.7 mm.

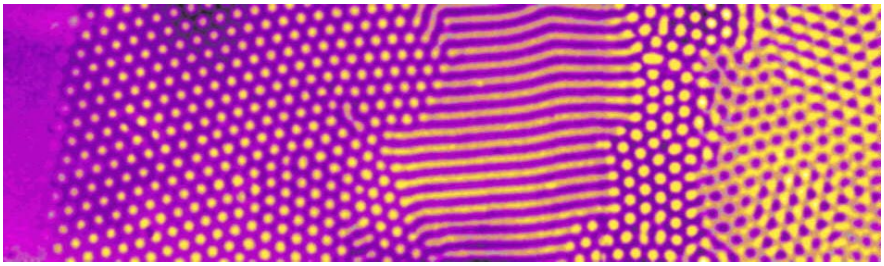

Fig. 4. Unfolded sequence of patterns in a bevelled disc two-side-fed reactor (TSFR): The thickness of the disc (diameter 21 mm) increases from left to right, from 1.7 mm to 3.2 mm. Feed conditions as in Fig. 2. View size 10.4×3.2 mm.

The transitions between all these new patterns are relatively smooth: patches of coexistent planforms are observed close to the pattern transition regions. The actual status of such unusual reaction–diffusion planforms is still a matter of debate. Even if it is clear that the third dimension can play an essential role in the development of these patterns, it is unclear if they are the result of mere moiré effects due to the superposition of layers of standard hexagon and stripe planforms [Bestehorn, 1996] or if these unusual planform symmetries correspond to genuine new solutions of quasi-2D systems. Another example of nonstandard planform is that of the so-called "black-eye" hexagonal patterns [Gunaratne *et al.*, 1994; Gomes, 1999]. These could be explained either by the activation of the over-

tones of the hexagon modes or as a projection of a 3D body-centered cubic pattern correctly oriented by the anisotropic effect of the feeding ramps.

The three-dimensional characteristics of patterns are difficult to resolve experimentally. Different indirect approaches have been attempted. By gradually dyeing the patterns in the thickness, Ouyang *et al.* [1992] show that, in a TSFR, the strong gradient of parameters seems to favor the stacking of two-dimensional patterns rather than the genuine three-dimensional structures predicted for uniform conditions by theory. Other experiments carried on with bevelled disc reactors (where the circular feed faces make an angle) confirm these results [Dulos *et al.*, 1996; Rudovics *et al.*, 1996]. The latter experiments show that the distance between the feed surfaces not only acts on the thickness Δ of the pattern stratum, so that one or more layers of patterns can develop, but it also plays the role of a bifurcation parameter. As the thickness of the disc increases, a sequence of patterns develops (Fig. 4) exhibiting a transition from a uniform state to an hexagonal array of clear spots, then another transition to parallel stripes.

This corresponds to the standard pattern sequence predicted by theory of two-dimensional systems. Beyond the domain of stripes, a new domain of clear hexagons follows: this is an example of reentrant hexagons which can be accounted for by different theoretical approaches [Verdasca *et al.*, 1992; Dewel *et al.*, 1995; Dufiet & Boissonade, 1996]. Then follow domains with the nonstandard triangles and hexa-bands planforms. This supports the interpretation that these exotic planforms result from the superposition of patterns spread in two layers. Triangles would result from the superposition of clear hexagons of the first layer with dark hexagons of the second layer, while hexa-bands would correspond to the superposition of stripes and dark hexagons. Indeed, numerical simulations [Borckmans *et al.*, 1992; Setayeshgar & Cross, 1998, 1999] show that, in the presence of parameter gradients, patterns with different symmetries can develop at different locations along the gradients. It is however noteworthy that, in experiments, the invoked dark hexagon patterns, were never observed as asymptotic monolayer patterns [Dulos *et al.*, 1996; Ouyang & Swinney, 1991] which may question their origin in "multilayer structures".

The use of two-side-fed reactors has also allowed for the study of spatiotemporal patterns found in region III (Fig. 2). At high malonic acid concentration, the chemical reaction–diffusion system exhibits traveling waves [Fig. 5(a)] with very

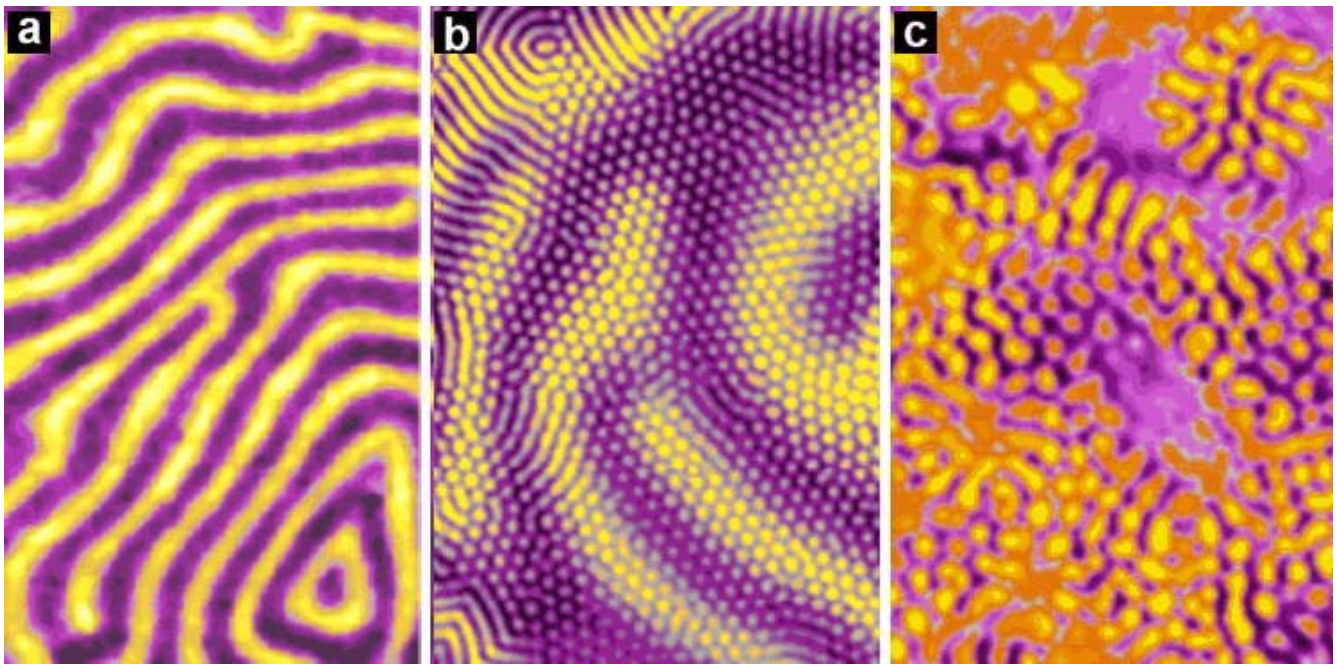

Fig. 5. Spatiotemporal structures observed in the different subregions III of Fig. 2. (a) Wave pattern (region IIIa), (b) superposition of a stationary hexagonal array of clear spots and traveling waves (region IIIc), (c) chaotic Turing–Hopf mixed mode (region IIIb). View sizes (a) 10.6×17.0 mm; (b) 4.8×7.3 mm; (c) 2.7×4.0 mm.

poorly defined wavelength and quite uniform period. The wavelength of these traveling waves are nearly one order of magnitude greater than that of the neighboring Turing patterns.

These are phase waves that can spontaneously break and form spirals rotating with the same period as the rest of the wave pattern. This differs from triggered waves in excitable media where spirals always tend to induce a frequency higher than that of the spontaneous bulk relaxation oscillations [Zykov, 1987]. The transition from the stationary patterns of region II to the plane wave state of region IIIa [Fig. 5(a)] can be directly along the MP portion of the Hopf bifurcation line or indirectly through a series of complex spatiotemporal behaviors where both wave- and Turing-like patterns are associated. The direct transition is sharp and, as mentioned above, exhibits no detectable hysteresis. Involved spatiotemporal dynamics such as Turing–Hopf mixed-modes (spatial patterns oscillating in time), localized structures (a stationary spatial structure imbedded into an oscillating bulk or vice-versa) [Perraud *et al.*, 1993; Heidemann *et al.*, 1993] as well as more complex or even chaotic dynamics have been predicted theoretically to appear close to a codimension-two Turing–Hopf point [Kidachi, 1980; De Wit *et al.*, 1993, 1996]. It is defined as the point in parameter space where the thresholds of both Turing and Hopf instabilities coincide. Experimentally, one observes that above the codimension-two Turing–Hopf point M, two different mixed mode states exist: in subregion IIIc, the mixed mode appears as a stationary hexagon pattern over which waves are superimposed [Fig. 5(b)]; the two modes seem to interact very weakly in this region of control parameter. In contrast, waves and Turing-like patterns strongly interact in subregion IIIb. This new spatiotemporal structure is characterized by a less ordered Turing mode superimposed by irregular waves and scattered with "smooth state holes", the latter dominated by the sole oscillatory Hopf mode. Figure 5(c) provides a snapshot of such a spatiotemporal structure which is an example of a chaotic Turing–Hopf mixed-mode.

In a TSFR, the thickness Δ of the patterned stratum cannot be directly controlled. The large changes in chemical concentrations and in stoichiometric ratio of species between the two feed surfaces make difficult both interpretation of the experimental results and quantitative modeling since most of the tractable kinetic models are usually valid over restrained ranges of concentrations.

2.2. *One-side-fed reactors (OSFR)*

To avoid some of the above mentioned difficulties, experiments are now usually performed in one-side-fed reactors (OSFR) sketched in Fig. 1(b). In these reactors, the CST-2 of Fig. 1(a) is replaced by an impermeable transparent wall and all chemicals are introduced in the same tank that now becomes a genuine continuously stirred tank reactor (CSTR). The disc of the gel is pressed against the impermeable wall and the opposite face is in contact with the contents of the CSTR. Often, as presented here, an inorganic membrane is placed between the disc and the CSTR in order to rigidly maintain the disc of gel. Moreover, this membrane may introduce some decoupling between the dynamics of the CSTR contents and that of the gel, as we shall discuss later. The disc of the gel is very thin (e.g. a typical thickness of 0.2 mm). Consequently, it is often considered that no significant concentration gradient would develop through the thickness of the gel. Since this corresponds to a disc thickness of the order or less than the wavelength of the pattern, these reactors are often thought of as good approximations of extended two-dimensional systems irrespective of chemical feed concentrations. Another advantage of such reactors is that they also allow for direct correlations to be made between the dynamics of the CSTR and that of the gel.

The dynamics of such a device is described [Blanchedeau *et al.*, 2000] by the following set of equations respectively for the CSTR and the gel:

$$\frac{\partial \mathbf{c}_\mathrm{s}}{\partial t} = f(\mathbf{c}_\mathrm{s}) + \frac{(\mathbf{c}_0 - \mathbf{c}_\mathrm{s})}{\tau} + \rho_V \frac{D}{e}\left(\frac{\partial \mathbf{c}}{\partial z}\right)_{z=0}, \qquad (7)$$

$$\frac{\partial \mathbf{c}}{\partial t} = f(\mathbf{c}) + D\nabla^2 \mathbf{c}\,, \qquad (8)$$

where $\mathbf{c}_0$, $\mathbf{c}_\mathrm{s}$ and $\mathbf{c}$ are the concentrations of the species respectively in the input flow, in the CSTR, and inside the gel, D is the corresponding diffusion coefficient, τ the residence time of the CSTR, e is the thickness of the gel, ρ_V the ratio of the volume of the gel to the volume of the CSTR, and z is the normal direction to the CSTR/gel interface. The f's are the reaction rates. On the right-hand side of Eq. (7), the second term represents the input and output flows of the species. It contains all the expandable control parameters of the system. The third term results from the diffusive flux of the species at the interface between the gel and the

CSTR and represents the feedback of the gel contents on the CSTR dynamics. When the volume of the CSTR is large with regard to the volume of the gel ($\rho_V \ll 1$), this last term can usually be neglected so that the chemical state of the CSTR is independent of the state of the gel and the concentrations in the CSTR act as a Dirichlet boundary condition for Eq. (8) at $z = 0$ (in contact with the CSTR), whereas a no-flux boundary condition is applied at $z = e$ (along the impermeable wall).

Whatever the dynamics in the gel, the CSTR can exhibit any behavior of homogeneous nonlinear dynamical systems such as multistabilities, oscillations or even chaotic behaviors. In the experiments presented here, we have not considered the regions of parameters where the CSTR becomes self-oscillatory in order to avoid the more intricate situation of periodically forced spatiotemporal systems.

Lengyel *et al.* [1990a, 1990b] have shown that, when the CIMA reaction oscillates, most of the initial chlorite and iodide ions have been consumed and that the major species are then chlorine dioxide, iodine and malonic acid. These are the reagents of the CDIMA reaction. The following results for OSFR were obtained by operating this CDIMA reaction in the CSTR, in regions of parameters where the reacting solution does not oscillate and can therefore only be in a monostable stationary state. For appropriate feed compositions, the standard sequence, predicted by theory, of two-dimensional hexagonal and stripe patterns is observed, similarly to what was observed for monolayers in the TSFR. Here however, the dimensionality of the pattern is directly controlled by the designed parameters of the reactor. The phase diagrams of Fig. 6 were established step by step, using the malonic acid concentration as the bifurcation parameter [Rudovics *et al.*, 1999]. From left to right, one can distinguish three types of regions: (i) a region of uniform stationary state, (ii) a region of stationary hexagonal and stripe Turing patterns, (iii) a region of oscillations in the CSTR for which corresponding dynamics in the gel was disregarded.

Faithful modeling, using the reduced seven variable kinetic LE-model of the CDIMA reaction proposed by Lengyel and Epstein [1992] is used [Rudovics *et al.*, 1999] to determine the CSTR dynamics and concentrations. At the same time, taking advantage that, in the CDIMA reaction, the initial reactants can be in stoichiometric excess relative to dynamical variables such as I^- and ClO_2^-, a "pool-chemical approximation" for the initial species can be made for the gel part (i.e. the concentration of the initial species are maintained fixed and uniform over space). This is a very attractive way to reduce the computational model to account for the reaction–diffusion instabilities in the gel. Pattern calculations can thus be reduced to that of a two variable system in a two-dimensional space. Considering the extreme simplicity of the model compared to the actual chemical kinetics, the agreement between computational and experimental results is very satisfactory both at the level of the Turing and Hopf limits and at that of the pattern distributions and wavelength dependence as a function of control parameters.

As seen above, thin one-side-fed reactors can act as good approximation of extended two-dimensional systems. From this point of view, the thinner the gel, the better the two-dimensional approximation should be. A thickness equal to or less than the wavelength, as it is the case in the experiments reported here, would seem appropriate but a new problem then arises. At the feed interface of the gel, the concentration of all species is actually maintained constant and uniform by contact with the CSTR. This defines uniform Dirichlet boundary conditions in the vicinity of which no pattern

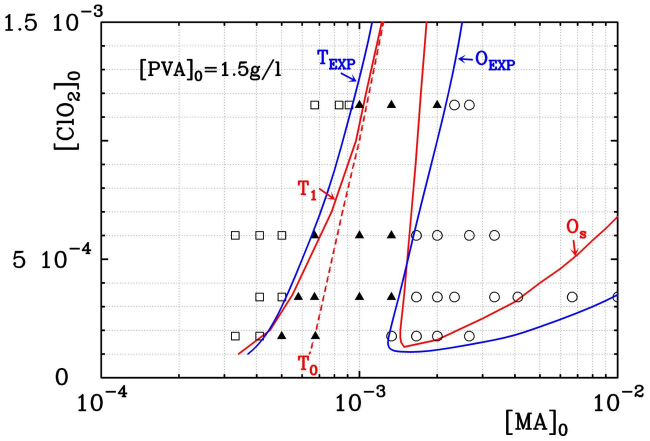

Fig. 6. Experimental and computed phase diagrams obtained with the CDIMA reaction operated in a one-side-fed reactor (OSFR). Section in the ($[MA]_0$, $[ClO_2]_0$) plane. MA = malonic acid; Experimental observations (red): white square: Stationary uniform states; black triangle: Turing patterns; white circle: Oscillatory states; thin full line: Limit of Turing (T_{EXP}) and oscillatory (O_{EXP}) domains (estimated from these data). Numerical simulations (blue); thick short dashed lines: Turing bifurcation (T_0); thick long dashed lines: Limit of bistability between uniform and patterned states (T_1); thick full line: Limit of oscillatory domain (O_S).

can form. In thin gels, the influence of the boundary conditions should spread over the whole gel and hinder all transverse instabilities (i.e. parallel to the feed surface). How can patterns then develop in experiments performed in a thin OSFR? As a matter of fact, the contact between the gel and the CSTR is achieved through a membrane. This membrane, together with the turbulent fluid boundary layer which necessarily develops at the contact between the membrane and the CSTR, effectively reduces the efficiency of exchanges between the gel and the bulk of the CSTR. This introduces some partial decoupling between the contents of the CSTR and the gel, and acts as mixed boundary conditions. The latter conditions have different consequences for two classes of species: the major reagents and the intermediate dynamical species. Whereas this effect is small on the concentrations of the slowly consumed input species (which are in excess), these conditions are close to no-flux conditions for the intermediate rapidly changing species involved in the formation of the Turing patterns [Rudovics *et al.*, 1999]. Thus, the patterns are let free to develop in the plane parallel to the feed-faces. Notice that, the 2D pool chemical approximation is only valid when such time scale separation between feed species and dynamical species is made possible. This type of situation is only found in chemical systems which allow for transient batch oscillatory dynamics over some range of initial concentrations.

3. Bistable Systems

As mentioned in the introduction, reaction–diffusion type systems may exhibit several coexisting HSS for the same set of parameters and different diffusive instabilities issued from these HSS may interact. What then becomes of the standard pattern selection problem? Experiments have revealed that similar sequences of structures occur in physically different diffusive systems when they exhibit bistability between HSS [Firth *et al.*, 1992; Ackemann *et al.*, 1995; Breazeal *et al.*, 1995]. This suggests that a theoretical analysis of the pattern selection on a model reaction–diffusion system could capture the highlights of bifurcation diagrams in general bistable reaction–diffusion type systems. As an illustration, let us consider a two-variable Fitzhugh–Nagumo (FHN) reaction–diffusion model featuring bistability between HSS and characterized by the competition between an activator x and an inhibitor y:

$$\frac{\partial x}{\partial t} = x - x^3 - y + \beta xy + \nabla^2 x\,, \tag{9}$$

$$\frac{\partial y}{\partial t} = \xi(\gamma x - y - a) + \delta\nabla^2 y\,, \tag{10}$$

where $\delta = D_y/D_x$ is the ratio of the diffusion coefficients and $\xi = \tau_x/\tau_y$ that of the characteristic time scales of the two fields. These equations were initially derived as a simple model for the conduction of the action potential along unmyelinated nerve axons [Murray, 1993]. The analysis of its dynamics has however proved useful to autocatalytic chemistry on numerous occasions since it played a key role in the systematic design of chemical oscillators [Boissonade & De Kepper, 1980] or in describing chemical wave propagation when the medium is excitable [Tyson & Keener, 1988; Zykov, 1987] instead of being bistable. We take $\xi > 1$ to avoid the presence of Hopf bifurcations as in the experiments mentioned at the beginning of this section. We distinguish two parameters a and γ that control the relative position and the number of intersections between the nullclines. $\beta \neq 0$ characterizes the breaking of the ($x \to -x$, $y \to -y$, $a \to -a$) symmetry.

Turing patterns

Let us first consider the symmetric $\beta = 0$ case. When $a = a_c = 0$ and $\gamma = \gamma_c = 1$, the system exhibits a critical point (cusp). Around this point, the model possesses either one or three HSS. When a is taken as control parameter and $\gamma < 1$, bistability emerges through two back-to-back saddle-node bifurcations at $a = a_{sn}^{\pm}$, creating a symmetric hysteresis loop based on the two HSS $(x_{\pm}, y_{\pm})$ stable with respect to uniform perturbations. A third unstable HSS results from the reconnection of the unstable manifolds arising from the saddle-node bifurcations. When the spatial processes are taken into account, diffusive instabilities may appear symmetrically on both HSS at $a = a_T^{\pm}$, respectively on x_+ and x_-. This information is summarized in Fig. 7(a), where, for given ξ and δ, we have represented the locus of the homogeneous saddle-node bifurcations $(a_+\gamma_c a_-)$ together with that of the diffusive instabilities $(X_+\gamma_T X_-)$ in the (a, γ) parameter space. For a given $\gamma = \gamma_0$, these loci determine $a = a_{sn}^{\pm}$ and $a = a_T^{\pm}$. For $\gamma < \gamma_L$, no more Turing instabilities appear on the HSS. Nevertheless, isolated

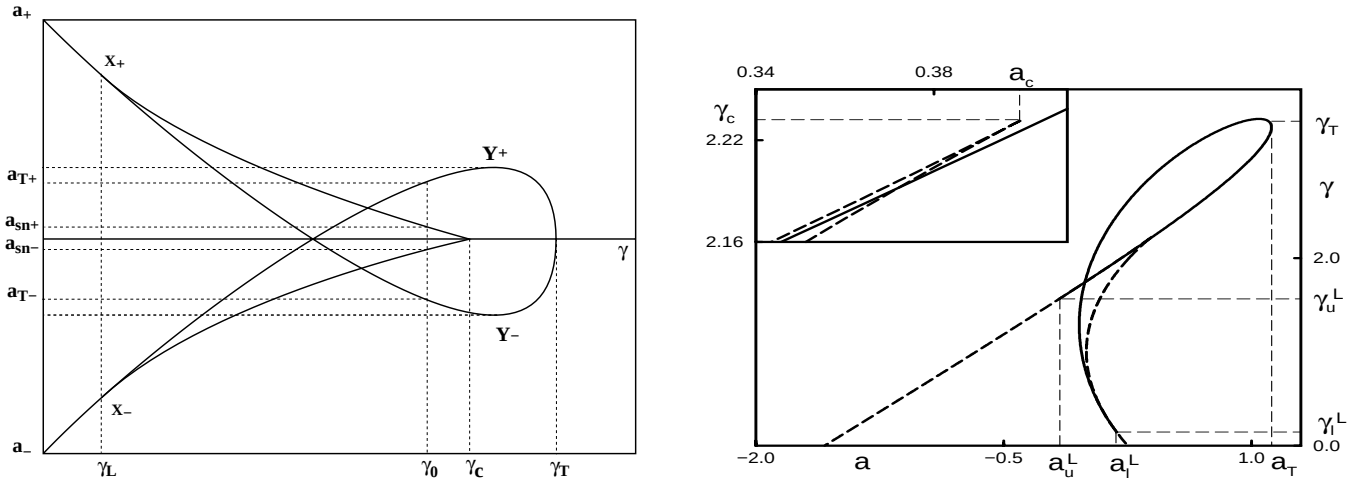

(a) (b)

Fig. 7. Schematic phase space $(a;\gamma)$ for the FitzHugh–Nagumo model (for fixed ξ and δ in the absence of Hopf bifurcations). The locus of the homogeneous saddle-node bifurcations is represented by the curve $(a_+\gamma_c a_-)$ originating from the cusp γ_c. (a) Symmetric case $\beta = 0$. The locus of Turing instabilities is given by $(X_+\gamma_T X_-)$. (b) Asymmetric case $\beta \neq 0$. The locus of Turing instabilities is given by $(\gamma_u^L \gamma_T \gamma_l^L)$. The inset enlarges the region near the cusp.

branches of Turing patterns remain possible [Vastano, 1987; Métens *et al.*, 1997]. The system can be analyzed in the vicinity of the critical point and we thus essentially discuss the situation of nascent bistability.

Our analysis relies on the fact that the homogeneous perturbations around the uniform states are quasi-neutral. As a consequence, a *zero mode* is activated by the saddle-node bifurcations and must be taken into account in the dynamics since it will compete with the spatial active modes and thereby affect the amplitudes and the stability of the patterns. This zero mode essentially gives rise to new types of resonant contributions [Dewel *et al.*, 1995]. We therefore approximate the concentration fields $\mathbf{c}$ by a linear superposition of these active modes

$$\mathbf{c} = \mathbf{e}_1 A_0 + \left[\mathbf{e}_2 \sum_{i=1}^{M} A_i \exp(i\mathbf{q_i}\cdot\mathbf{r}) + c.c.\right], \quad (11)$$

where ($|\mathbf{q_i}| = q_c$), $\mathbf{e}_1$ and $\mathbf{e}_2$ are the eigenvectors of the Jacobian matrix of the homogeneous and distributed systems. In 2D, for the case of the resonant patterns ($M = 3$ with $\mathbf{q}_1 + \mathbf{q}_2 + \mathbf{q}_3 = 0$), the reduction to a center unstable manifold [Roberts, 1985] leads to coupled amplitude equations [Métens *et al.*, 1997]:

$$\partial_t A_0 = h(A_0) + \alpha \sum_{i=1}^{3} |A_i|^2 - \beta_1 \sum_{i=1}^{3} |A_i|^2 A_0 - \beta_2 (A_1^* A_2^* A_3^* + A_1 A_2 A_3) \quad (12)$$

$$\partial_t A_1 = \mu A_1 + \alpha[A_0 A_1 + A_2^* A_3^*] - g_1 |A_1|^2 A_1 - g_2[|A_2|^2 + |A_3|^2] A_1 - g_3 A_1 A_0^2 - g_4 A_0 A_2^* A_3^* \quad (13)$$

with $h(A_0) = (\gamma - 1)A_0 - A_0^3$ and cyclic permutations (c.p) of the subscripts for the equations of A_2 and A_3. We consider only the case of a cubic nonlinearity saturation (β_1, β_2, g_3, g_4 are positive). The growth rate μ of the critical modes is computed from the linear stability analysis. The amplitude equations admit the following classes of solutions: (i) homogeneous solutions given by $h(A_0) = 0$ with $A_1 = A_2 = A_3 = 0$ corresponding to the reference states (HSS); (ii) patterned solutions for which the amplitudes of both types of modes are different from zero. They may exhibit either smectic, i.e. stripes, ($A_0 \neq 0$, $|A_1| \neq 0$, $|A_2| = |A_3| = 0$ and c.p) or hexagonal ($A_0 \neq 0$, $|A_1| = |A_2| = |A_3| \neq 0$) symmetries. In the smectic case, Eqs. (12) and (13) admit three solutions for the homogeneous component, A_0, represented by the inverted S branch labeled A_s in Fig. 8(a). In contrast to the case of the HSS, it is only the intermediate part of the branch that is stable. The corresponding amplitudes of the inhomogeneous components $R_s = |A_1|$ are given in Fig. 8(b). Solutions of hexagonal symmetry ($A_0 = A$, $A_i = R_i e^{i\phi_i}$, $i = 1, 2, 3$) are again determined by the total phase $\Phi = \phi_1 + \phi_2 + \phi_3$ of the resonant modes. According to the sign of $v^* = g_4 A - \alpha$, the stable stationary value of Φ is

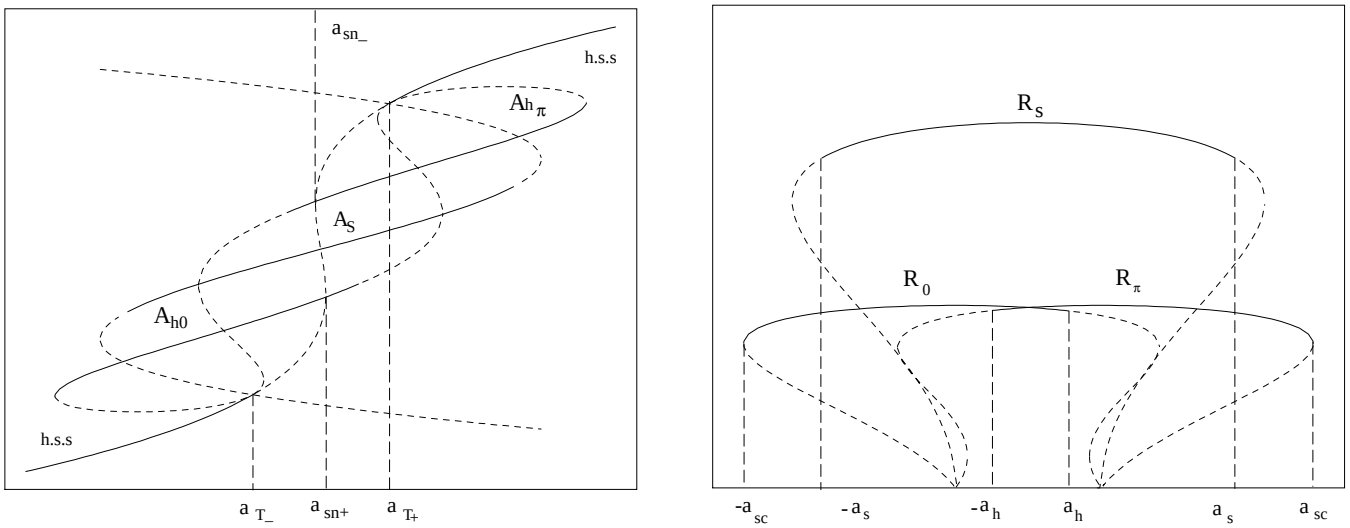

(a) (b)

Fig. 8. Bifurcation diagram in the bistable region for the FHN model with a as parameter. (a) Amplitudes of the homogeneous components of the stripe (A_s) and hexagonal ($A_{h\pi}$, A_{h0}) patterns. The homogeneous steady states are shown by the thicker lines. (b) Moduli of the amplitudes of the corresponding modulated components of the same structures (R_s: stripes, R_0 and R_π: hexagons). Stable states are in full lines. h_0 and h_π are, respectively, stable in the ranges $[-a_{sc}, a_h]$ and $[-a_h, a_{sc}]$. The stripes are stable in the interval $[-a_s, a_s]$.

zero ($v < 0$) or π ($v > 0$). These values correspond respectively to a triangular (h_0) or a honeycomb (h_π) lattice. For each value of Φ, we again find a triplet of solutions as shown in Fig. 8(a) by the two inverted S labeled A_{h0} and $A_{h\pi}$ linking the two Turing instability points. Again the intermediate parts are the stable ones. The corresponding inhomogeneous components are represented in Fig. 8(b).

The relative stability of the striped and hexagonal patterns is also taken into account in Fig. 8. These bifurcation diagrams are in agreement with the results of our numerical integration of this FHN model. On varying parameter a, one observes the sequence $\mathrm{HSS}_1 \leftrightarrow h_{0(\pi)} \leftrightarrow$ stripes $\leftrightarrow h_{\pi(0)} \leftrightarrow \mathrm{HSS}_2$. This succession is typical of bistable systems and is experimentally observed in a large diversity of systems [Firth *et al.*, 1992; Ahlers, 1993; Ackemann *et al.*, 1995; Breazeal *et al.*, 1995].

The principal property that distinguishes the behavior of bistable systems, with respect to strictly monostable systems, arises from the effects of the homogeneous mode that acts globally on the dynamics through its resonant coupling with the spatial active modes. It ensures that patterns are obtained with amplitudes that are of the order of the difference in amplitudes between (x_+, y_+) and (x_-, y_-). Such large-amplitude patterns cannot be described by applying the standard weakly nonlinear analysis around a_T^+ or a_T^-. The pseudoquadratic coupling v^* involving the zero mode induces large subcriticality of h_0 and h_π, respectively to the left of a_T^- and to the right of a_T^+. The stripes also appear subcritically. As a result, large domains of coexistence between hexagons, stripes and the HSS can be observed. In these regions, stable stationary localized structures like hexagonal domains of h_0 or h_π embedded in the uniform state can be obtained numerically. Spatial coexistence of structures of different symmetries is also possible; for instance both types of hexagons may coexist [Dewel *et al.*, 1995].

For the symmetric FHN model discussed above, the branches of patterned solutions issued from the two Turing instabilities interconnect. However, most experimental systems do not exhibit this nongeneric property of symmetry. In the nonsymmetric case, the critical wave numbers q_c^u and q_c^l are different. This has interesting consequences as we shall summarize now.

To study this case, one sets $\beta \neq 0$ in Eqs. (9) and (10). An increase of the asymmetry parameter β induces a distortion of the hysteresis loop in the (x (or y), a) plane. In the presence of a differential diffusion process ($\delta > 1$), each of the HSS can be destabilized by inhomogeneous perturbations. In general, two Turing instabilities are created, one on the upper and the other one on the lower HSS. In the (a, γ)-plane [Fig. 7(b)], when γ is decreased below γ_T, they migrate, invade the cusp region and

approach the limit points. For a given value of γ, the diffusive instability comes closest to the saddle-node bifurcation whose curvature $K_i(i = u, l)$ is the largest and the corresponding wavenumber the smallest. In the FHN model, one has $K_u > K_l$, and thus $q_c^u < q_c^l$. The Turing bifurcation on the upper branch of the activator x is also the first to come in coincidence with the limit point at $\gamma = \gamma_u^L$. For $\gamma < \gamma_u^L$, the pattern-forming instability only appears on the lower branch and when $\gamma < \gamma_l^L$, no more diffusive instability occurs on the HSS. To derive the corresponding amplitude equations the set of active modes must now contain those arising from both Turing instabilities as well as the zero mode related to bistability of the HSS (M and N modes related to the Turing instabilities, respectively on the upper and lower HSS).

To avoid being too technical, we refer the reader to [Bachir *et al.*, 2001], and shall not write down the corresponding amplitude equations deriving from the decomposition on the active modes:

$$\mathbf{c} = \mathbf{e}_1 A_0 + \left[\mathbf{e}_2 \sum_{i=1}^{M} A_i \exp(i\mathbf{q}_i \cdot \mathbf{r}) + \mathbf{e}_3 \sum_{j=1}^{N} B_j \exp(i\mathbf{q}_j \cdot \mathbf{r}) + c.c \right] . \quad (14)$$

The results of this analysis is that, first of all, the model exhibits the standard striped and hexagonal patterns of wave numbers q_c^u and q_c^l that arise, respectively from the Turing instabilities on the upper and lower HSS. In the asymmetric case,

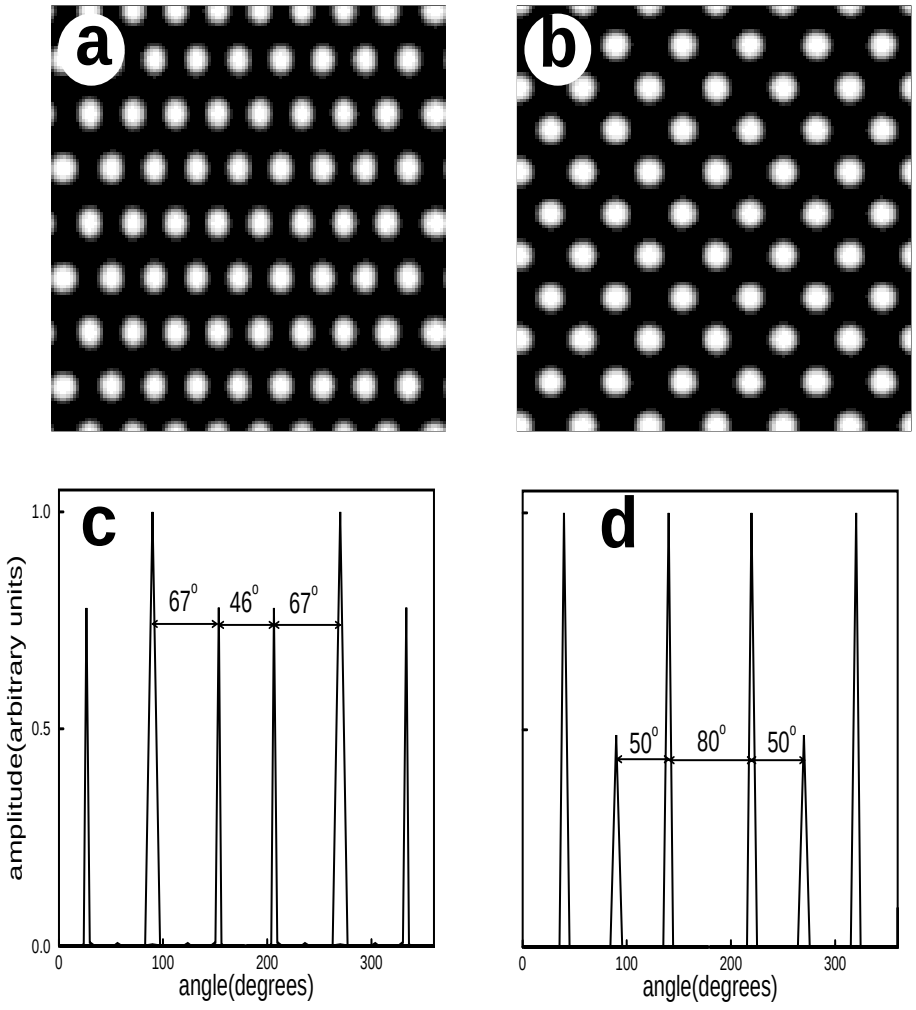

Fig. 9. 2D rhombic patterns obtained by numerical integration of the FHN model [Eqs. (9) and (10)] with $a = -0.1$, $\beta = 0.7$, $\gamma = 0.9$, $\xi = 2.5$ and $\delta = 120$. (a and b) Rhombs corresponding to the cases when the sum of the phases of the modes $\Phi = 0$. (c and d) Angular amplitude distribution in spatial frequency space for the patterns in (a) and (b), respectively.

these branches *do not reconnect* with each other. Moreover new resonant interactions between active modes associated with the two Turing instabilities can occur. The simplest correspond to two families (Fig. 9) of rhombic patterns ($M = 1$, $N = 2$ or $M = 2$, $N = 1$) corresponding to isoceles triangles in q-space $\mathbf{q}_1^l + \mathbf{q}_2^l + \mathbf{q}_3^u = 0$ or $\mathbf{q}_1^u + \mathbf{q}_2^u + \mathbf{q}_3^l = 0$ and which may have been observed experimentally [Ouyang *et al.*, 1993]. These resonant patterns should not be confused with the unstable rhombic planforms characterized by two critical wavenumbers of length q_c^i ($i = u$ or l) and making an angle such that their sum does not correspond to an active mode. There, contrary to the case of the isoceles triangles, the phases of the active modes are arbitrary. The rhombs considered here can coexist with the regular hexagons in the vicinity of the instability points.

Furthermore, when the critical wave numbers q_c^u and q_c^l become sufficiently different, superlattice structures can also be generated through the combination in q-space of various resonant triplets, either equilateral or isoceles. An example is given in Fig. 10 corresponding to an equilateral triangle decorated by three isoceles triangles in q-space ($M = 3$, $N = 6$): $\mathbf{q}_1^l + \mathbf{q}_2^l + \mathbf{q}_3^l = 0$, $\mathbf{q}_1^l + \mathbf{q}_1^u + \mathbf{q}_2^u = 0$, $\mathbf{q}_2^l + \mathbf{q}_3^u + \mathbf{q}_4^u = 0$ and $\mathbf{q}_3^l + \mathbf{q}_5^u + \mathbf{q}_6^u = 0$. The resulting pattern is composed of two discrete but interacting sublattices and thus presents a spatial order on two different length scales. Such dynamic superlattices have also been obtained in nonlinear optical devices [Pampaloni *et al.*, 1997; Musslimani & Pismen, 2000] and in two-frequencies Faraday experiments [Kudrolli *et al.*, 1998; Arbell & Fineberg, 1998]. Finally, for specific relations between the angles of the triads of wave vectors of active modes, quasiperiodic patterns may also be generated. All these new structures thus appear as *self-induced resonances* resulting from the interaction between two different symmetry-breaking instabilities. The spatial modes associated to one of the diffusive instabilities play the role of a forcing on the other (and vice-versa).

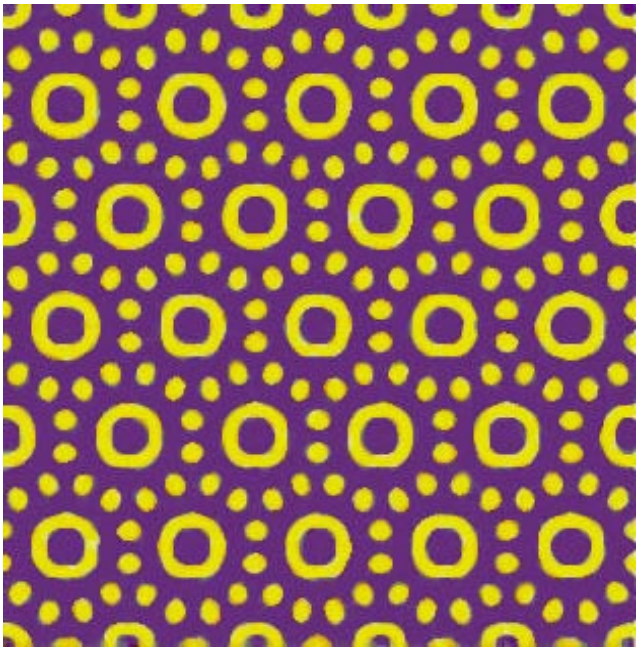

Fig. 10. Superlattice Turing pattern obtained from a numerical integration of the FHN model [Eqs. (9) and (10)] for $\beta = 0.7$, $\gamma = 0.9$, $\xi = 2.5$ and $\delta = 120$.

As a final remark, we must point out that the mechanisms presented in the preceding paragraphs are still operative in the purely monostable region close to the cusp point.

Front patterns

But this is not the whole story about pattern formation in bistable HSS systems. Indeed, precisely because two different HSS are both stable for the same set of parameters, another important class of solutions can be constructed. It consists in a front linking the two HSS, thereby separating the system into two adjoining spatial regions: one where HSS_1 exists, the other containing HSS_2. Such fronts, the detailed properties of which depend on the characteristics of the reaction–diffusion system at hand, have been well studied in the past (e.g. [Ortoleva & Ross, 1975; Pismen, 1979]). Under differential diffusion conditions, similar to those met for the Turing pattern formation, such fronts may undergo a class of morphological instabilities that were first described by Kuramoto [1984]. It was further extensively studied in relation to pattern formation by Hagberg and Meron [1994a, 1994b] and shown to be able to lead to the development of labyrinthine-type patterns as in Fig. 11. These instabilities should not be confused with the front instabilities that are for instance involved in the nucleation of Turing structures in monostable systems, such as the CDIMA system [Davies *et al.*, 1998]. There, the front behind which the structure emerges, invades the unstable HSS after quenching the system beyond b_T and bistability of HSS is not involved. The thresholds of Turing and front instabilities differ from one another and may eventually

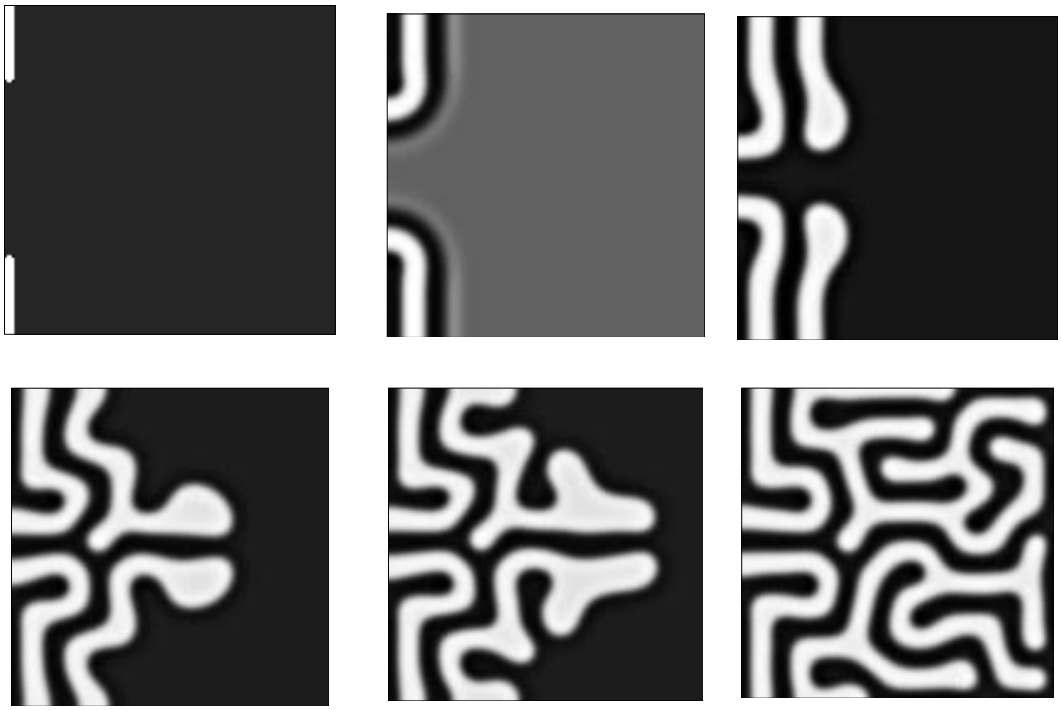

Fig. 11. Development of a labyrinthine pattern in the FHN model [Eqs. (9) and (10)] through a morphological instability of a front connecting the two HSS (black and white).

compete. Therefore, the pattern that results depends on the basin of attraction to which the initial conditions belong. This competition between labyrinthine and Turing structures is still a matter of research. Recently, it has been shown on a particular dynamical system, a variant of the Swift–Hohenberg model [Cross & Hohenberg, 1993], that a bifurcation is involved in this transition [Di Menza *et al.*, 2001]. In this intricate domain, a lot of investigations are still needed both from the theoretical and experimental view points. Labyrinthine patterns have been observed [Lee *et al.*, 1993; Lee & Swinney, 1995; Li *et al.*, 1996] in an OSFR operated with the ferrocyanide-iodate-sulphite (FIS) reaction [Edblom *et al.*, 1986]. Numerical integrations of a reaction–diffusion model based on a possible skeleton kinetic mechanism of this reaction lead to numerous patterned behaviors that were observed, which include the labyrintine structures [Lee & Swinney, 1995]. These numerical results were built on the now called CFUR approximation [Vastano *et al.*, 1987, 1988]. In this approximation, the gel part of the OSFR is assimilated to a two-dimensional reaction–diffusion system where each point is directly fed by fresh reactants, and releases all the species involved in the kinetic mechanism. The system is thus described as a 2D-continuum of CSTRs coupled by diffusion and its dynamics is described by

$$\frac{\partial \mathbf{c}(\mathbf{r},\, t)}{\partial t} = \mathbf{f}(\mathbf{c},\, b) + \frac{(\mathbf{c}_o - \mathbf{c})}{\tau} + D\nabla^2\mathbf{c}(\mathbf{r},\, t) \quad (15)$$

Under such formulation, the two first terms of Eq. (15) may give rise to bistability of HSS. Thus, in the CFUR approximation, Turing and front instabilities and their resulting patterns may be generated as discussed previously in this section using for instance the FHN model. However, here lies a snag because autocatalytic reactions in solution chemistry generally exhibit bistability of HSS only under CSTR-type feed conditions and the gel part of the OSFR is not fed in such a way. Indeed, the kinetic part of Eq. (8) does not give rise to bistability of HSS on its own. The CSTR bistability finds its origin in presence of the second (feeding) term of Eq. (7) or (15). A term that is not operating in the gel part. What more likely occurs in an OSFR is discussed in the next part.

4. Spatial Bistability

In view of the discussion at the end of the previous paragraph, let us briefly recall the bases of

bistability in a CSTR. If the input flow rate is large — that is if the residence time is much shorter than the typical reaction time — the extent of reaction is small and, in the stationary regime, the concentrations are close to the composition in the input flow ("flow state" F). If the residence time is much longer than the reaction time, the composition inside the reactor is close to that of the thermodynamic equilibrium that one would obtain in a closed reactor with the same initial concentrations ("thermodynamic state" T). In standard reactions, the branches of flow and thermodynamic states are smoothly connected at intermediate flow rates, but when autocatalytic or similar nonlinear kinetic processes are present, the two states can both exist for a same set of flow rates defining two distinct branches F and T. Many examples of this well known "temporal bistability" can be found in reference books [Field & Burger, 1985; Epstein & Pojman, 1998]. Most reactions which are bistable in a CSTR exhibit "clock dynamics" in batch, that is a sudden single switch to a state close to equilibrium after a well defined induction period, characterized by a low conversion rate. The switch occurs when the concentration of some species involved in the positive feedback loop process reaches a critical level. Thereafter, the conversion rate considerably speeds up. In these reactions, after the dynamical switch, at least one of the major initial reactants is nearly totally consumed. Consequently, when modeling these reaction systems, the feed terms cannot be eliminated even at the lowest level of approximation. In these conditions, no "pool chemical" approximation is possible for all input species at the same time. Therefore, whereas the study of a clock reaction in the CFUR approximation can be mapped onto the FHN model considered before, this cannot be done for the gel part of an OSFR.

A detailed analysis of pattern development in a bistable system was developed in the framework of the chlorine dioxide–iodide (CDI) reaction. This reaction belongs to the family of the CIMA and CDIMA reactions that lead to Turing patterns, as seen above. It is a "minimal" nonlinear chemical system [Epstein & Orbán, 1985; De Kepper *et al.*, 1990] for which a very comprehensive kinetic mechanism has been proposed [Lengyel *et al.*, 1996] which quantitatively accounts for the batch and CSTR dynamical behaviors of the reaction. This prototypic bistable reaction system is less complex and has a much better established kinetic mechanism than that of the bistable FIS reaction which has led to the observation of labyrinthine and other interacting front patterns [Lee *et al.*, 1993; Li *et al.*, 1996] in a disc OSFR slightly more intricate than the one described in Fig. 1(b).

4.1. *Propagating fronts in a disc shaped OSFR*

In batch conditions, the chlorine dioxide–iodide (CDI) reaction exhibits a typical "clock" behavior. When operated in a CSTR, this reaction can exhibit both sustained oscillations and bistability. As for the previous iodide-driven reactions of the family, polyvinyl alcohol (PVA) may be used as an iodine–iodide color indicator. As a matter of fact, because the iodine–iodide–PVA colored complex is inert in the reaction process, PVA is not only a color indicator but it can also control the effective reactivity of iodide, the activatory species. In the following experiments, this effect was used to expand the domain of bistability at the expense of the region of oscillations [Blanchedeau *et al.*, 2000].

The following results were obtained when operating the CDI reaction in a disc OSFR, of the type sketched in Fig. 1(b), fed with chemicals in 3% weight PVA solutions. The CSTR dynamics can exhibit bistability between two HSS over the range of $[I^-]_0$ values between 1.25 and 2.25×10^{-3} M. The HSS reached high values of $[I^-]_0$ and the colored reddish purple corresponds to the F state while the other HSS, reached a low $[I^-]_0$ and colored pale yellow corresponds to the T state.

In the OSFR, with the CSTR part in the T state, the disc of gel is uniformly pale yellow, thus the gel also belongs to the T state branch. At high iodide concentration, the CSTR is in the F state and the gel is uniformly reddish purple. The gel remains in the F state as $[I^-]_0$ is decreased until it reaches a critical value close to the low limit of the bistability domain. Just beyond this $[I^-]_0$ critical value, another less colored state appears in the gel. This new state starts invading the disc from the rim while the CSTR remains in the F state. If $[I^-]_0$ is further decreased, the new state in the disc disappears while the contents of the CSTR undergoes the transition to the pale yellow T state. If, on the contrary $[I^-]_0$ is increased, the new state is maintained in the gel up to another critical value where the gel switches back to the darker F state. Thus, bistability of steady states is observed for the gel for 1.26×10^{-3} M $\leq [I^-]_0 \leq 2.00 \times 10^{-3}$ M.

When a front is created between these two steady states, the rate and the direction of propagation as well as the morphology of this front sensitively depend on $[I^-]_0$. For $[I^-]_0 = 1.8 \times 10^{-3}$ M, the "clearer state" invades the F state [Figs. 12(a)–12(c)] and the propagation rate increases as $[I^-]_0$ is decreased (see Table 1). While for $[I^-]_0 = 1.8 \times 10^{-3}$ M the propagating front is smooth (Fig. 12), at lower values of $[I^-]_0$, the front loses its smoothness. Ondulations develop with increasing amplitude and decreasing average wavelength, as $[I^-]_0$ is lowered (Table 1) (Fig. 13). This is the result of a transversal morphological instability [Kuramoto 1984; Scott & Showalter 1992; Horváth *et al.*, 1993; Horváth & Showalter, 1995; Toth *et al.*, 1996]. For $[I^-]_0$ higher than $1.8\ 10^{-3}$ M, say 1.9×10^{-3} M as in Figs. 12(d)–12(f), the direction of propagation of the front is reversed, the darker state invades the clearer one. Note that, consequently to such a $[I^-]_0$ increase, made just after the snapshot of Fig. 12(c), the front slows down, stops and reverses. However, this reversal in the propagation direction does not occur simultaneously for all parts of the front around the dark state dropplet. The flatter parts of the front

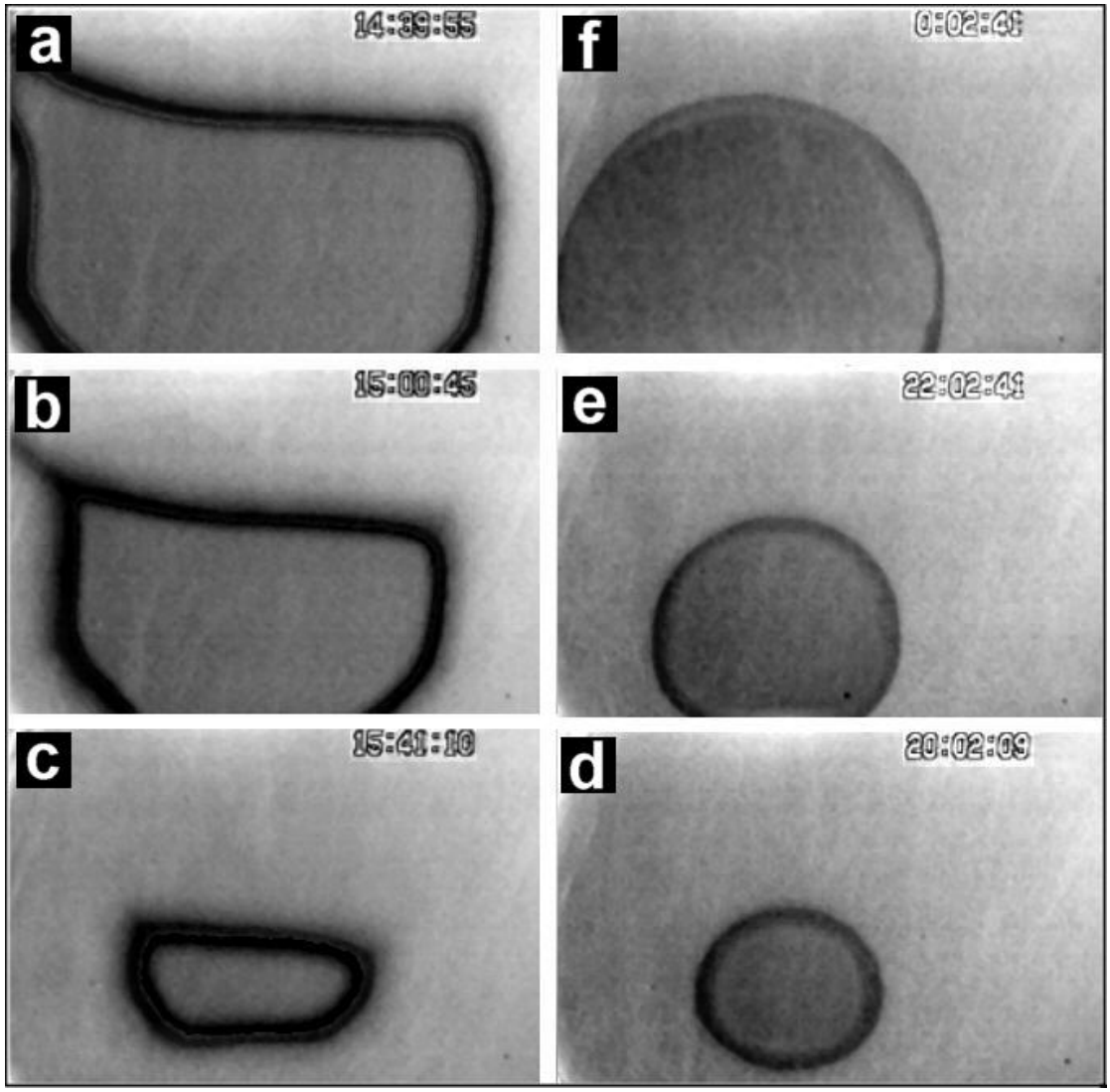

Fig. 12. Time sequence of a front propagation observed in a disc shaped one-side-fed reactor operated with the bistable CDI reaction: Initial state: reactor fed with $[I^-]_0 = 2 \times 10^{-3}$ M. Front observed 30 min after a jump in $[I^-]_0$ feeding from 2×10^{-3} M to 1.8×10^{-3} M; (a–c) front propagation sequence, time interval between two successive snapshots $\simeq$ 30 min, (d) front shape 4h after changing $[I^-]_0$ from 1.8×10^{-3} M to 1.9×10^{-3} M just after snapshot *c*; (c–e) front propagation sequence in the inverse direction, time interval between two successive snapshots $\simeq$ 120 min. Fixed parameters: $[ClO_2]_0 = 3.84 \times 10^{-4}$ M, residence time of the CSTR 8 min, temperature 25^0C.

Table 1. Front rate and characteristic wavelength of indentations.

$[I^-]_0$ (mM)	Front velocity (mm/h)	Average λ (mm)
1.8	2.1	smooth
1.7	3.6	1.0
1.6	5.3	0.71
1.5	9.6	0.43

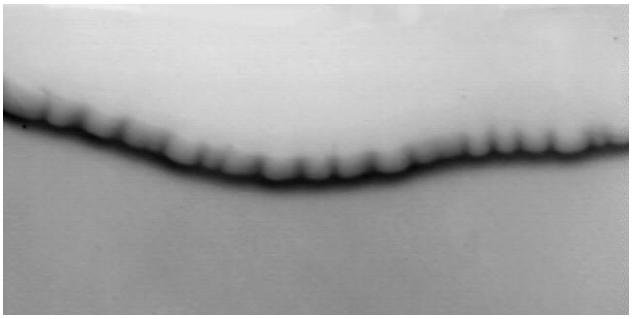

Fig. 13. Transversal front instability in the CDI reaction operated in a disc shaped one-side-fed reactor (OSFR). Initial conditions as in Fig. 12. Front observed after a finite concentration jump in $[I^-]_0$ from 2×10^{-3} M to 1.5×10^{-3} M.

reserve first and, as a result, the droplet takes a circular shape [Fig. 12(d)]. This infers that the direction of front propagation may depend on curvature and that, in this new direction [Figs. 12(d)–12(f)], the rate increases with decreasing curvature.

In the above described experiments, two different states can coexist in the gel for the same boundary conditions at the gel/CSTR interface over times longer than the diffusion time of species through the gel. One would like to understand how the continuity of these two states is ensured in the thickness of the disc of gel. In other words, how are the concentration changes organized in the depth of the gel? Observations in the disc shaped OSFR do not allow for the determination of such concentration profiles. The only directly available information is the total light absorption integrated across the thickness of the disc.

4.2. *Propagating fronts in a ring shaped OSFR*

Ring shaped OSFRs, as sketched in Fig. 14, were designed in order to directly acquire information on the concentration profiles in a direction corresponding to the thickness of the disc of gel [Blanchedeau *et al.*, 2000]. This OSFR is made of

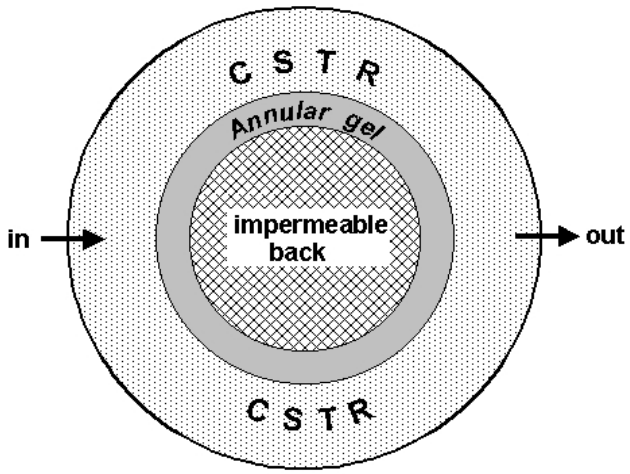

Fig. 14. Schematic representation of an annular strip OSFR. Outer diameter of the gel annulus = 15 mm; e is the distance between the outer and inner diameters of the annulus. Three different annulus were used with $e = 0.5$, 1.0 and 2.0 mm.

a flat ring of agarose gel fed from its external edge in contact with the contents of a CSTR. The other sides are pressed against impermeable walls. The width e of the ring is equivalent to the thickness of the previous disc of gel. Observations are made from above, perpendicularly to the feed direction. As before, the reactor is fed with solutions of chemicals of the CDI reaction and the agarose gel is loaded with PVA. The reacting solution in the CSTR exhibits bistability as a function of the iodide concentration. The two branches of the bistable respectively correspond to the T and F states and their limits are respectively called L_T and L_F.

Taking into account the state of the CSTR, three different states of the whole system can be distinguished, as a function of feed concentrations. If the CSTR contents corresponds to the T branch, the gel is uniformly pale yellow: this defines, as in the previous section, the T state of the gel. If the CSTR contents belongs to the flow branch, the gel can either be in a uniform reddish-purple color (defining the F state of the gel) or exhibit a sharp color switch from reddish-purple, on the CSTR side, to pale yellow, deeper in the ring of gel. In the following, this mixed state of the gel will be referred as the FT state. The latter two cases are illustrated in Figs. 15(a) and 15(b). The two different gray scale profiles correspond respectively to the dark and clearer states in the disc OSFR.

The domains of stability of these states and the transitions between them were determined by decreasing or increasing $[I^-]_0$. They are reported in

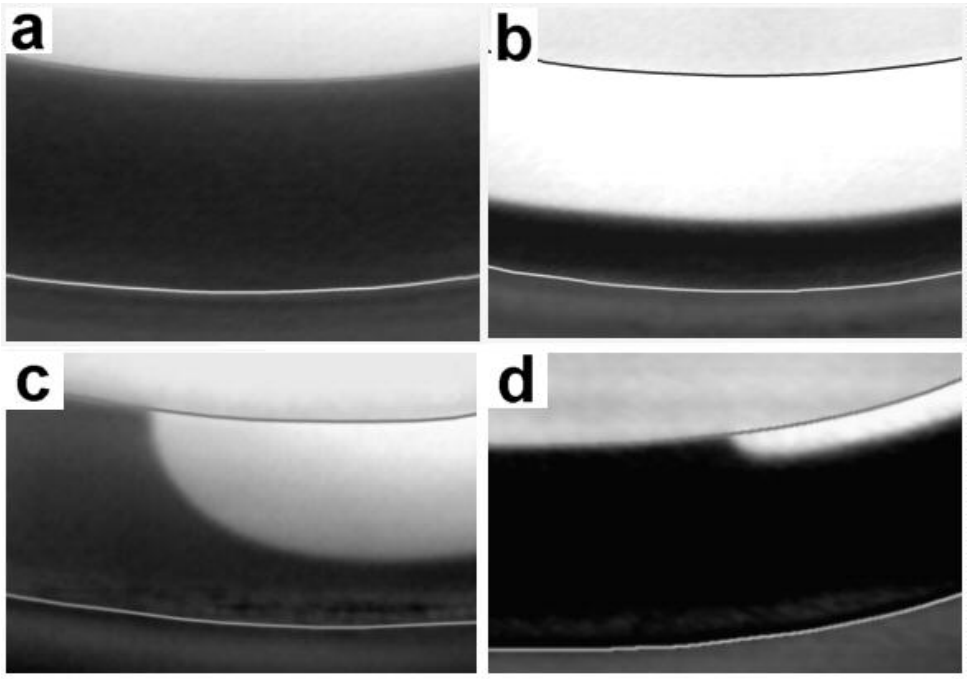

Fig. 15. Spatial bistability in the annular strip OSFR. (a) F state; (b) FT state; (c and d) interface between the F and FT states. The arc-lines are the limits of the gel. The lower arcs delineate the CSTR/gel interface, the upper arcs delineate the impermeable wall. Distance between the two arc-lines, $e = 1$ mm; values of $[I^-]_0 = 1.24\times10^{-3}$ M in (a–c); $[I^-]_0 = 1.25\times10^{-3}$ M in (d).

Fig. 16(B) for different values of e. At high and low $[I^-]_0$, the F and T states are respectively the only possible stable states. As expected, in the intermediate range of $[I^-]_0$, the domain of stability of the three states can overlap and give rise to bistability or tristability. The extent of these overlaps sensitively depends on e. The F state loses stability before the critical L_F value is reached. While for e=0.5 mm, the two transition values cannot be distinguished, the differences between them increase with the gel thickness. At low $[I^-]_0$, the FT state gives place to a T state as the contents of the CSTR switches to the thermodynamic branch. Within our experimental accuracy, this limit does not significantly depend on e. At high $[I^-]_0$, the FT state ends with a transition to state F. This transition is gradually shifted to higher $[I^-]_0$ when e increases. Limiting ourselves to the case where the CSTR remains on the F branch, the region of overlapping F and FT states determines what we call the region of spatial bistability [Blanchedeau *et al.*, 2000]. The extent of the spatial bistability decreases when e increases from 0.5 to 2 mm.

Model calculations based on the detailed scheme proposed by Lengyel *et al.* [1996] and taking into account the actual experimental setting (i.e. gel of thickness e diffusively connected to a CSTR) were performed [Blanchedeau *et al.*, 2000]. The computed phase diagram presented in Fig. 16(B) is in quasi-quantitative agreement with the experimental results [Fig. 16(A)]. In particular, the right domain of spatial bistability is obtained. At $e =$ 2.0 mm, the domain of spatial bistability is vanishingly small. However, this domain extends slightly beyond L_T, contrary to experimental observations. Calculations also predict that spatial bistability should disappear when $e < e_{\text{inf}}$. It is even shown that below a critical value, $e < e_{\text{inf}} = 0.039$ mm, no mixed state can be observed, whatever the value of $[I^-]_0$. Such small e values could not be reached in experiments for technical reasons.

In experiments, in the domain of parameters where both F and FT are stable, it is possible to produce an interface between these two states [Figs. 15(c) and 15(d)] and to study their relative stability as a function of the control parameter. The interface between the two states can be made to move in one or the other direction by finely adjusting the $[I^-]_0$ value. Note that the characteristics (i.e. the relative extensions of the F and T parts)

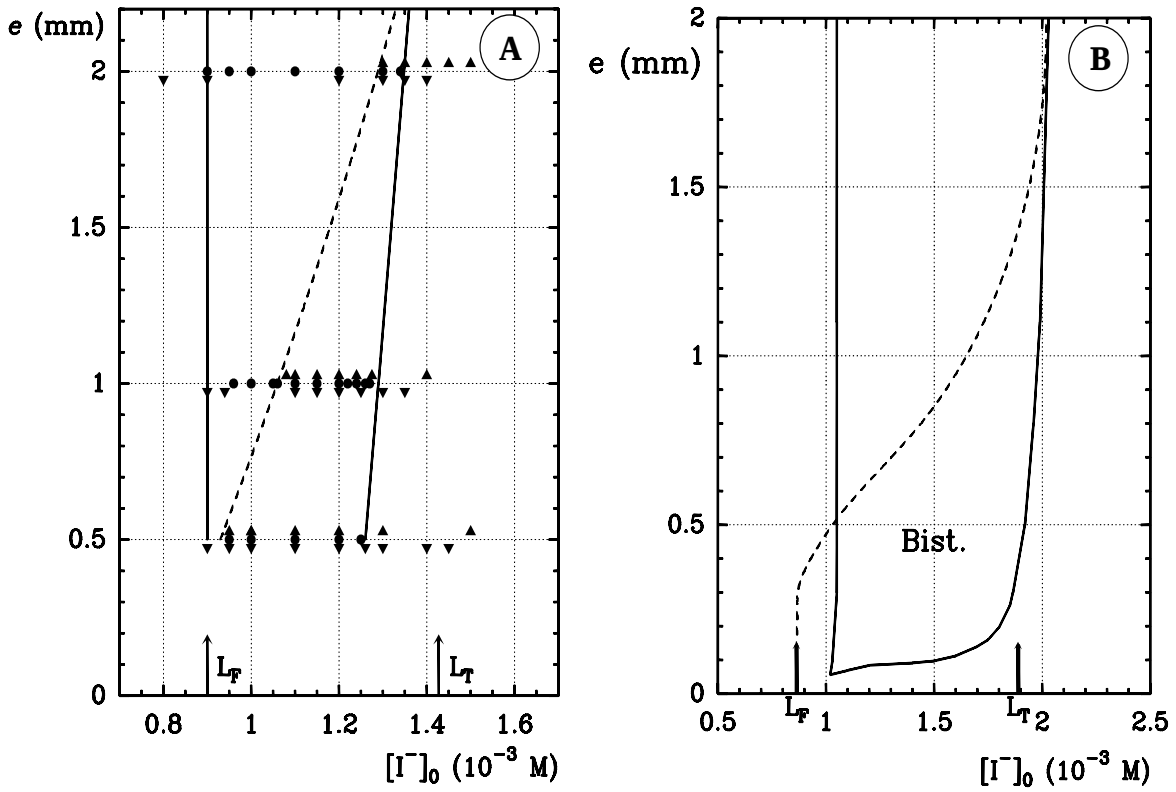

Fig. 16. Phase diagrams and spatial bistability in the plane (e, $[I^-]_0$). Full lines are the lower and upper $[I^-]_0$ limits of the FT state. Dotted lines are the minimum $[I^-]_0$ values for which the F state is stable. Spatial bistability lays in between this latter limit and the upper FT state limit. (A) Experimental results: the symbols correspond to the experimental points at $e = 0.5$, 1.0 and 2.0 mm (up triangles: F state; down triangles: T state; bullets: FT state). (B) Numerical results: residence time of the CSTR 10^3 s.

of the mixed state and correlatively those of the interface between this state and the F state of the gel can sensitively depend on control parameter values. Thus, as illustrated in Figs. 15(c) and 15(d) the change in the propagation direction of the F/FT interface comes with a change in the aspect ratio of this interface in the thickness, a phenomenon also found in model calculations [Blanchedeau & Boissonade, 1998]. These observations clearly show that even in thin disc OSFR, the now most popular spatial reactor design, the third dimension can seldom be discarded to account for the dynamics and the pattern mode selection mechanisms.

5. Conclusions

We have focused the present review on Turing structures formation in connection with the various types of reactors used in experiments. Emphasis was put on the differences that result from the use of chemical reaction systems which either exhibit bistability of HSS or solely a single HSS in a CSTR. The literature on periodic pattern formation through diffusive instabilities is so vast that covering all aspects is beyond the scope of this brief review. In the context of Turing pattern formation in chemical reaction–diffusion systems, we may refer the reader to other reviews focused on the monostable case, the Turing–Hopf interaction and localized patterns in TSFRs [Boissonade *et al.*, 1995; Ouyang & Swinney, 1995; Borckmans *et al.*, 1995; De Wit, 1999] and in batch reactors [Lengyel & Epstein, 1995].

As a conclusion, we wish to draw the reader's attention on a few other works related to Turing structures and to other regular pattern formation mechanisms that have recently been brought to light.

Despite the successes garnered since the first experimental demonstration of Turing patterns, it is fair to admit that very few chemical systems have led to Turing patterns or their likes. Therefore, the field is always on the lookout for promising new reactions [Orbán *et al.*, 2001] or media that would favor periodic pattern formation. Recently, the latter type of approach was remarkably and successfully

exemplified by operating the well known Belousov–Zhabotinsky reaction in a water-in-oil microemulsion [Vanag & Epstein, 2001]. In these conditions, a wealth of standing and traveling patterns that were undocumented in this reaction could be produced. In this quest, one must still beware of convection that is always lurking as stressed by the ongoing debate around the patterns observed in the methylene blue-sulfide-oxygen system [Watzl & Münster, 1995; Kurin-Csörgei *et al.*, 1998, 1999; Münster, 1999; Orbán *et al.*, 1999]. In this and other cases, further effects may have to include the coming into play of the mechanical changes that occur in the material supporting the reaction (e.g. the gel matrix) [Steinbock et al., 1998].

In other respects, the sensitivity to light of chemical reactions can be used to control the spatial structures and apprehend some of their properties through spatially uniform illumination, constant or periodic in time [Horvath *et al.*, 1999; Dolnik *et al.*, 2001a, 2001b; Sanz-Anchelergues *et al.*, 2001].

Spatial symmetry breaking can also occur through other mechanisms. Symmetry breaking takes place through the strong resonant forcing of spatially distributed oscillators as was theoretically proposed by Coullet and Emilsson [1992a, 1992b] and finally experimentally observed and studied [Petrov *et al.*, 1997; Lin *et al.*, 2000]. Nonlocal feedbacks imposing long-range inhibition may readily give rise to pattern formation [Hildebrand *et al.*, 2001; Mikhaïlov, 1994; Middya *et al.*, 1993] when competing with some short-range activation process. Systematic studies of the spatial unfolding of elementary bifurcations have recently been set out by Coullet *et al.* [2000]. These aim at answering questions such as: are the homogeneous bifurcations anticipated by another bifurcation when spatiotemporal perturbations are introduced and what is the nature of the eventually created patterns? They consider all generic codimension one bifurcations in dimension smaller or equal to 2 that include, on the one hand, saddle-node and Hopf bifurcations of fixed points, and saddle-node of cycles and homoclinic bifurcations for periodic orbits on the other hand.

Besides the labyrinthine patterns, discussed previously, the FIS reaction also generated stationary or oscillating Turing structures through a transient spot self-replication mechanism starting from a localized trigger [Lee *et al.*, 1994]. A similar dynamics was also observed with the CDIMA reaction [De Kepper *et al.*, 1994; Davies *et al.*, 1998]. A prototypical model is that of the irreversible "autocatalator" [Gray & Scott, 1990] which, in a CFUR description, exhibits a large variety of behaviors [Pearson, 1993]. As revealed by extensive numerical work, these behaviors include self-replicating spots that generate various asymptotic states in 2D, as well as pulses that self-replicate in 1D. For this model, self-replication is observed in the vicinity of a Takens–Bogdanov point when diffusion of species is introduced. This complex problem has recently received a fair amount of attention. Although precise mathematical elements of response about the origin of the phenomenon are becoming known in 1D, it is not yet clear whether, in 2D, symmetry breaking of the spots in the azimuthal direction is also involved. In order not to overload the reference list, we refer the reader to an overview paper by Nishiura and Ueyama [1999]. In a way, these theoretical works are in line with the concept of spatial unfolding of bifurcations considered by Coullet *et al.* [2000]. Here however, the bifurcation in the absence of spatial effects is of codimension two! The generality of the Nishiura and Ueyama explanation remains to be assessed as spot replication was also observed numerically for the Brusselator model where a Takens–Bogdanov point is not present [Tlidi *et al.*].

One point worth coming back to is the statement that hydrodynamical flows are systematic hindrances to regular pattern formation! Quite to the contrary, in tubular plug flows, the differential flow induced chemical instability (DIFICI) [Rovinsky & Menzinger, 1992] and the flow distributed oscillators (FDO) patterning mechanisms [Kuznetsov *et al.*, 1997; Andresén *et al.*, 1999, 2000], first proposed theoretically, were subsequenly supported by experimental observations [Rovinsky & Menzinger, 1993; Kaern & Menzinger, 1999]. Whereas DIFICI gives rise to periodic traveling waves, FDO may lead to periodic stationary patterns, even when the diffusion coefficients of the activator and inhibitor are equal. The FDO model seems to appeal to biologists as it is able to produce various repeated or periodic patterns in cellularized growing tissues [Kaern *et al.*, 2000a, 2000b; Jaeger & Goodwin, 2001].

Having transited to the realm of biology, we have, in some sense, gone a full circle as Turing's ideas were introduced to try to account for some aspects of morphology in biology. This domain, fertilized by the recent discoveries of genetics, is of an even wider scope, too wide to even be set

ajar. Although the diffusing morphogen species remained elusive for a long time, things seem to be changing as discussed in the papers presented by Harland [2001] and Vincent and Perrimon [2001]. The use of reaction–diffusion type systems, implementing mechano-chemical properties of cells is for instance discussed in the works by Meinhardt [Meinhardt, 1994; Koch & Meinhardt, 1994] and Murray [1993]. Reaction-transport equations are now even finding a place in the description of the heterogeneous nature (microtubules and molecular motors) of cells as shown in the work of Lee and Kardar [2001] and the references there cited. To quote Murray: "Although genes play a crucial role in the control of pattern formation, genetics says nothing about the actual mechanism involved nor how the vast range of pattern and form that we see evolves from an homogeneous mass of dividing cells". We are modestly hoping that the work discussed in this review can contribute to the understanding of such great schemes.

Acknowledgments

The review includes work obtained in collaboration with M. Bachir, E. Barillot, P. Blanchedeau, P. W. Davies, V. Dufiet, M. F. Hilali, D. Lima, S. Métens, B. Rudovics and J. A. Verdasca.

We thank the F.N.R.S. (Belgium), the Van Buuren Foundation (Belgium) and C.N.R.S. (France) for their support. The collaborative work between the ULB and the CRPP was also sponsored through CGRI-FNRS/CNRS and Tournesol grants.

References

Ackemann, T., Logvin, Yu. A., Heuer, A. & Lange, W. [1995] "Transition between positive and negative hexagons in optical pattern formation," *Phys. Rev. Lett.* **75**, 3450–3453.

Ahlers, G., Berge, L. I. & Cannell, D. S. [1993] "Thermal convection in the presence of a first-order phase change," *Phys. Rev. Lett.* **70**, 2399–2402.

Andresén, P., Bache, M., Mosekilde, E., Dewel, G. & Borckmans, P. [1999] "Stationary space-periodic structures with equal diffusion coefficients," *Phys. Rev.* **E60**, 297–301.

Andresén, P., Mosekilde, E., Dewel, G. & Borckmans, P. [2000] "Comment on flow-distributed oscillations: Stationary chemical waves in a reacting flow," *Phys. Rev.* **E62**, 2992–2993.

Arbell, H. & Fineberg, J. [1998] "Spatial and temporal dynamics of two interacting modes in parametrically driven surface waves," *Phys. Rev. Lett.* **81**, 4384–4387.

Arecchi, F. T., Boccaletti, S. & Ramazza, P. [1999] "Pattern formation and competition in nonlinear optics," *Phys. Rep.* **318**, 1–83.

Bachir, M., Métens, S., Borckmans, P. & Dewel, G. [2001] "Formation of rhombic and superlattice patterns in bistable systems," *Europhys. Lett.* **54**, 612–618.

Bestehorn, M. [1996] "Two layer model showing a variety of pattern types near nonequilibrium phase transitions," *Phys. Rev.* **E53**, 4842–4846.

Blanchedeau, P. & Boissonade, J. [1998] "Resolving an experimental paradox in open spatial reactors: The role of spatial bistability," *Phys. Rev. Lett.* **81**, 5007–5010.

Blanchedeau, P., Boissonade, J. & De Kepper, P. [2000] "Theoretical and experimental studies of spatial bistability in the chlorine-dioxide-iodide reaction," *Physica* **D147**, 283–299.

Boissonade & De Kepper, P. [1980] "Transition from bistability to limit cycle oscillations. Theoretical analysis and experimental evidence in an open chemical system," *J. Phys. Chem.* **84**, 501–506.

Boissonade, J., Dulos, E. & De Kepper, P. [1995] "Turing patterns: From myth to reality," in *Chemical Waves and Patterns*, eds. Kapral, R. & Showalter, K. (Kluwer, Dordrecht), pp. 221–268.

Borckmans, P., De Wit, A. & Dewel, G. [1992] "Competition in ramped Turing structures," *Physica* **A188**, 137–157.

Borckmans, P., Dewel, G., De Wit, A. & Walgraef, D. [1995] "Turing bifurcations and pattern selection," in *Chemical Waves and Patterns*, eds. Kapral, R. & Showalter, K. (Kluwer, Dordrecht), pp. 323–363.

Breazeal, W., Flynn, K. M. & Gwinn, E. G. [1995] "Static and dynamic two-dimensional patterns in self-extinguishing discharge avalanches," *Phys. Rev.* **E52**, 1503–1515.

Callahan, T. K. & Knobloch, E. [1996] "Bifurcations on the fcc lattice," *Phys. Rev.* **E53**, 3559–3562.

Callahan, T. K. & Knobloch, E. [1999] "Pattern formation in three-dimensional reaction–diffusion systems," *Physica* **D132**, 339–362.

Castets, V., Dulos, E., Boissonade, J. & De Kepper, P. [1990] "Experimental evidence of a sustained standing turing-type nonequilibrium chemical pattern," *Phys. Rev. Lett.* **64**, 2953–2956.

Coullet, P. & Emilsson, K. [1992a] "Pattern formation in the strong resonant forcing of spatially distributed oscillators," *Physica* **A188**, 190–200.

Coullet, P. & Emilsson, K. [1992b] "Strong resonances of spatially distributed oscillators: A laboratory to study patterns and defects," *Physica* **D61**, 119–131.

Coullet, P., Risler, E. & Vandenberghe, N. [2000] "Spatial unfolding of elementary bifurcations," *J. Stat. Phys.* **101**, 521–541.

Cross, M. C. & Hohenberg, P. C. [1993] "Pattern formation outside of equilibrium," *Rev. Mod. Phys.* **65**, 851–1112.

Davies, P. W., Blanchedeau, P., Dulos, E. & De Kepper, P. [1998] "Dividing blobs, chemical flowers, and patterned islands in a reaction–diffusion system," *J. Phys. Chem.* **102**, 8236–8244.

De Kepper, P., Epstein, I. R., Orbán, M. & Kustin, K. [1982] "Batch oscillations and spatial wave patterns in chlorite oscillating systems," *J. Phys. Chem.* **86**, 170–171.

De Kepper, P., Boissonade, J. & Epstein, I. R. [1990] "Chlorite-iodide reaction: A versatile system for the study of nonlinear dynamical behavior," *J. Phys. Chem.* **94**, 6525–6536.

De Kepper, P., Perraud, J. J., Rudovics, B. & Dulos, E. [1994] "Experimental study of stationary Turing patterns and their interaction with traveling waves in a chemical system," *Int. J. Bifurcation and Chaos* **4**, 1215–1231.

Dewel, G., Métens, S., Hilali, M. F., Borckmans, P. & Price, C. B. [1995] "Resonant patterns through coupling with a zero mode," *Phys. Rev. Lett.* **74**, 4647–4650.

De Wit, A., Dewel, G., Borckmans, P. & Walgraef, D. [1992] "Three-dimensional dissipative structures in reaction–diffusion systems," *Physica* **D61**, 289–296.

De Wit, A., Dewel, G. & Borckmans, P. [1993] "Chaotic Turing–Hopf mixed mode," *Phys. Rev.* **E48**, R4191–R4194.

De Wit, A., Lima, D., Dewel, G. & Borckmans, P. [1996] "Spatiotemporal dynamics near a codimension-two point," *Phys. Rev.* **E54**, 261–271.

De Wit, A., Borckmans, P. & Dewel, G. [1997] "Twist grain boundaries in three-dimensional lamellar Turing structures," *Proc. Nat. Acad. Sc.* (*USA*) **94**, 12765–12768.

De Wit, A. [1999] "Spatial patterns and spatiotemporal dynamics in chemical systems," *Adv. Chem. Phys.* **109**, 435–513.

Di Menza, L., Le Berre, M., Pomeau, Y., Ressayre, E. & Tallet, A. [2001] "Description de la bifurcation rouleaux-labyrinthes," in *4èmes Rencontres du Non Linéaire*, eds. Pomeau, Y. & Ribotta, R. (Institut Poincaré), pp. 255–259.

Dolnik, M., Berenstein, I., Zhabotinsky, A. M. & Epstein, I. R. [2001a] "Spatial periodic forcing of Turing structures," *Phys. Rev. Lett.* **87**, 238301.

Dolnik, M., Zhabotinsky, A. M. & Epstein, I. R. [2001b] "Resonant suppression of Turing patterns by periodic illumination," *Phys. Rev.* **E63**, 026101 (1–10).

Dufiet, V. & Boissonade, J. [1992] "Numerical studies of Turing pattern selection in a two-dimensional system," *Physica* **A188**, 158–171.

Dufiet, V. & Boissonade, J. [1996] "Dynamics of Turing pattern monolayers close to onset," *Phys. Rev.* **E53**, 4883–4892.

Dulos, E., Davies, P., Rudovics, B. & De Kepper, P. [1996] "From quasi-2D to 3D Turing patterns in ramped systems," *Physica* **D98**, 53–66.

Edblom, E. C., Orbán, M. & Epstein, I. R. [1986] "A new iodate oscillator: The Landolt reaction with ferrocyanide in a CSTR," *J. Am. Chem. Soc.* **108**, 2826–2830.

Emelyanov, V. I. [1992] "Generation, diffusion, deformational instabilities and formation of order defect structures on the surface of solids under the effect of strong laser beams," *Laser Phys.* **2**, 389–466.

Epstein, I. R. & Orbán, M. [1985] "Halogen-based oscillators in a flow reactor," in *Oscillating and Traveling Waves in Chemical Systems*, eds. Field, R. J. & Burger, M. (Wiley, NY), pp. 257–286.

Epstein, I. R. & Pojman, J. A. [1998] *An Introduction to Nonlinear Chemical Dynamics* (Oxford University Press).

Falta, J., Imbihl, R. & Henzler, M. [1990] "Spatial pattern formation in a catalytic surface reaction: The facetting of Pt(110) in $CO+O_2$," *Phys. Rev. Lett.* **64**, 1409–1412.

Field, R. J. & Burger, M. (eds.) [1985] *Oscillating and Traveling Waves in Chemical Systems* (Wiley, NY).

Firth, W. J., Scroggie, A. J. & McDonald, G. S. [1992] "Hexagonal patterns in optical bistability," *Phys. Rev.* **A46**, R3609–R3612.

Glansdorff, P. & Prigogine, I. [1971] *Thermodynamic Theory of Structure, Stability and Fluctuations* (Wiley, NY).

Gomes, M. G. M. [1999] "Black-eye patterns: A representation of three-dimensional symmetries in thin domains," *Phys. Rev.* **E60**, 3741–3747.

Gray, P. & Scott, S. K. [1990] *Chemical Oscillations and Instabilities* (Oxford, Clarendon Press).

Gunaratne, G. H., Ouyang, Q. & Swinney, H. L. [1994] "Pattern formation in the presence of symmetries," *Phys. Rev.* **E50**, 2802–2820.

Hagberg, A. & Meron, E. [1994a] "Pattern formation in nongradient reaction–diffusion systems: The effects of front bifurcations," *Nonlinearity* **7**, 805–835.

Hagberg, A. & Meron, E. [1994b] "Complex patterns in reaction–diffusion systems: A tale of two front instabilities," *Chaos* **4**, 477–484.

Haken, H. & Olbrich, H. [1978] "Analytical treatment of pattern formation in Gierer-Meinhardt model of morphogenesis," *J. Math. Biol.* **6**, 317–331.

Harland, R. M. [2001] "A twist on embryonic signaling," *Nature* **410**, 423–424.

Heidemann, G., Bode, M. & Pürwins, H.-G. [1993] "Fronts between Hopf- and Turing-type domains in a two-component reaction–diffusion system," *Phys. Lett.* **A177**, 225–230.

Hildebrand, M., Skodt, H. & Showalter, K. [2001]

"Spatial symmetry breaking in the Belousov–Zhabotinsky reaction with light-induced remote communication," *Phys. Rev. Lett.* **87**, 088303.

Horvath, A. K., Dolnik, M., Munuzuri, A. P., Zhabotinsky, A. M. & Epstein, I. R. [1999] "Control of Turing structures by periodic illumination," *Phys. Rev. Lett.* **83**, 2950–2953.

Horváth, D., Petrov, V., Scott, S. K. & Showalter K. [1993] "Instabilities in propagating reaction–diffusion fronts," *J. Chem. Phys.* **98**, 6332–6343.

Horváth, D. & Showalter, K. [1995] "Instabilities in propagating reaction–diffusion fronts of the iodate-arseneous acid reaction," *J. Chem. Phys.* **102**, 2471–2478.

Horváth, D. & Tóth, A. [1997] "Turing patterns in a single-step autocatalytic reaction," *J. Chem. Soc., Farad. Trans.* **93**, 4301–4303.

Hunding, A. & Sorensen, P. G. [1988] "Size adaptation of Turing patterns," *J. Math. Biol.* **27**, 27–39.

Jaeger, J. & Goodwin, B. C. [2001] "A cellular oscillator model for periodic pattern formation," *J. Theor. Biol.* **213**, 171–181.

Kaern, M. & Menzinger, M. [1999] "Experimental observation of stationary chemical waves in a flow system," *Phys. Rev.* **E60**, R3471–R3474.

Kaern, M. & Menzinger, M. [2000] "Reply to 'Comment on flow-distributed oscillations: Stationary chemical waves in a reacting flow'," *Phys. Rev.* **E62**, 2994–2995.

Kaern, M., Menzinger, M. & Hunding, A. [2000a] "A chemical flow system mimics waves of gene expression during segmentation," *Biophys. Chem.* **87**, 121–126.

Kaern, M., Menzinger, M. & Hunding, A. [2000b] "Segmentation and somitogenesis derived from phase dynamics in growing oscillatory media," *J. Theor. Biol.* **207**, 473–493.

Kapral, R. & Showalter, K. (eds.) [1995] *Chemical Waves and Patterns* (Kluwer Academic Publishers, Dordrecht).

Kerner, B. S. & Osipov, V. V. [1994] *Autosolitons* (Kluwer Academic Publishers, Dordrecht).

Kidachi, H. [1980] "On mode interactions in reaction–diffusion equation with nearly degenerate bifurcations," *Progr. Theor. Phys.* **63**, 1152–1169.

Koch, A. J. & Meinhardt, H. [1994] "Biological pattern formation: From basic mechanisms to complex structures," *Rev. Mod. Phys.* **66**, 1481–1507.

Krishan, K. [1980] "Kinetics of void lattice formation in metals," *Nature* **287**, 420–421.

Kudrolli, A., Pier, B. & Gollub, J. P. [1998] "Superlattice patterns in surface waves," *Physica* **D123**, 99–111.

Kuramoto, Y. [1984] *Chemical Oscillations, Waves and Turbulence*, in Springer Series in Synergetics, Vol. 19 (Springer-Verlag, Berlin).

Kurin-Csörgei, K., Orbán, M., Zhabotinsky, A. M. & Epstein, I. R. [1998a] "On the nature of patterns arising during polymerisation of acrylamide in the presence of the methylene blue-sulfide-oxygen oscillating reaction," *Chem. Phys. Lett.* **295**, 70–74.

Kurin-Csörgei, K., Orbán, M., Zhabotinsky, A. M. & Epstein, I. R. [1998b] "Reply to Comment on 'On the nature of patterns arising during polymerization of acrylamide in the presence of the methylene blue-sulfide-oxygen oscillating reaction'," *Chem. Phys. Lett.* **311**, 105–107.

Kuznetsov, S., Mosekilde, E., Dewel, G. & Borckmans, P. [1997] "Absolute and convective instabilities in a 1D Brusselator flow model," *J. Chem. Phys.* **106**, 7609–7616.

Lee, K. J., McCormick, W. D., Ouyang, Q. & Swinney, H. L. [1993] "Pattern formation by interacting chemical fronts," *Science* **261**, 192–194.

Lee, K. J., McCormick, W. D., Pearson, J. E. & Swinney, H. L. [1994] "Experimental observation of self-replicating spots in a reaction–diffusion system," *Nature* **369**, 215–218.

Lee, K. J. & Swinney, H. L. [1995] "Lamellar structures and self-replicating spots in a reaction–diffusion system," *Phys. Rev.* **E51**, 1899–1914.

Lee, H. Y. & Kardar, M. [2001] "Macroscopic equations for pattern formation in mixtures of microtubules and molecular motors," *Phys. Rev.* **E64**, 056113 (1–8).

Lengyel, I. & Epstein, I. R. [1990] "Modeling of Turing structures in the chlorite-iodide-malonic acid-starch reaction system," *Science* **251**, 650–652.

Lengyel, I., Rábai, I. & Epstein, I. R. [1990a] "Batch oscillation in the reaction of chlorine dioxide with iodine and malonic acid," *J. Am. Chem. Soc.* **112**, 4606–4607.

Lengyel, I., Rábai, I. & Epstein, I. R. [1990b] "Experimental and modeling study of oscillations in the chlorine dioxide-iodine-malonic acid reaction," *J. Am. Chem. Soc.* **112**, 9104–9110.

Lengyel, I. & Epstein, I. R. [1992] "A chemical approach to designing Turing patterns in reaction–diffusion systems," *Proc. Nat. Acad. Sci.* (*USA*) **89**, 3977–3979.

Lengyel, I. & Epstein, I. R. [1995] "The chemistry behind the first experimental chemical example of Turing patterns," in *Chemical Waves and Patterns*, eds. Kapral, R. & Showalter, K. (Kluwer, Dordrecht), pp. 297–322.

Lengyel, I., Li, J., Kustin, K. & Epstein, I. R. [1996] "Rate constants for reactions between iodine and chlorine species: A detailed mechanism of the chlorine dioxide-chlorite-iodide reaction," *J. Am. Chem. Soc.* **118**, 3708–3719.

Li, G., Ouyang, Q. & Swinney, H. L. [1996] "Transitions in two-dimensional patterns in a ferrocyanide-iodate-sulfite reaction," *J. Chem. Phys.* **105**, 10830–10837.

Li, Y.-J., Olosnovitch, J., Mazouz, N., Plenge, F., Krischer, K. & Ertl, G. [2001] "Turing-type patterns on electrode surfaces," *Science* **291**, 2395–2398.

Lin, A. L., Bertram, M., Martinez, K., Swinney, H. L., Ardelea, A. & Carey, G. F. [2000] "Resonant phase

patterns in a reaction–diffusion system," *Phys. Rev. Lett.* **84**, 4240–4243.

Lugiato, L. A., Brambilla, M. & Gatti, A. [1998] "Optical pattern formation," *Adv. Atom. Molecul. Opt. Phys.* **40**, 229–306.

Manneville, P. [1990] *Dissipative Structures and Weak Turbulence* (Academic Press, NY).

Meinhardt, H. [1994] "Biological pattern formation: New observations provide support for theoretical predictions," *Bioessays* **16**, 627–632.

Métens, S., Dewel, G., Borckmans, P. & Engelhardt, R. [1997] "Pattern selection in bistable reaction–diffusion systems," *Europhys. Lett.* **37**, 109–114.

Middya, U., Graham, M. D., Luss, D. & Sheintuch, M. [1993] "Pattern selection in controlled reaction–diffusion systems," *J. Chem. Phys.* **98**, 2823–2836.

Mikhailov, S. A. [1994] *Fundation of Synergetics I. Distributed Active Systems* (Springer Verlag, Berlin).

Münster, A. F. [1999] "Comment on the nature of patterns arising during polymerization of acrylamide in the presence of the methylene blue-sulfide-oxygen oscillating reaction," *Chem. Phys. Lett.* **311**, 102–104.

Murray, J. D. [1989] *Mathematical Biology* (Springer Verlag, Berlin).

Musslimani, Z. H. & Pismen, L. M. [2000] "Dynamic quasicrystalline patterns: Wave-mode-Turing-mode resonance with Turing-mode self-interaction," *Phys. Rev.* **E62** 389–396.

Newell, A. C, Passot, T. & Lega [1993] "Order parameter equations for patterns," *Ann. Rev. Fluid Mech.* **25**, 399–453.

Nicolis, G. & Prigogine, I. [1977] *Self-Organization in NonEquilibrium Systems* (Wiley, NY).

Nicolis, G. [1995] *Introduction to Nonlinear Science* (Cambridge University Press, Cambridge).

Niedernostheide, F. J., Dohmen, R., Willebrand, H., Schulze, H. J. & Pürwins, H. G. [1992] "Pattern formation in nonlinear physical systems with characteristic electric properties," in *Nonlinearity with Disorder*, eds. Abdullaev, K., Bishop, A. R. & Pneumatikos, S., Springer Proc. Phys., Vol. 67, pp. 282–309.

Nishiura, Y. & Ueyama, D. [1999] "A skeleton structure of self-replicating dynamics," *Physica* **D130**, 73–104.

Orbán, M., Kurin-Csörgei, K., Zhabotinsky, A. M. & Epstein, I. R. [1999] "Pattern formation during the polymerisation of acrylamide in the presence of sulfide ions," *J. Phys. Chem.* **B103**, 36–40.

Orbán, M., Kurin-Csörgei, K., Zhabotinsky, A. & Epstein, I. R. [2001] "A new chemical system for studying pattern formation: Bromate-hypophosphite-acetone-dual catalyst," *Farad. Discuss.* **120**, 11–19.

Ortoleva, P. & Ross, J. [1975] "Theory of propagation of discontinuities in kinetic systems with multiple time scales: Fronts, front multiplicity, and pulses," *J. Chem. Phys.* **63**, 3398–3408.

Ouyang, Q. & Swinney, H. L. [1991] "Transition from a uniform state to hexagonal and striped Turing patterns," *Nature* **352**, 610–612.

Ouyang, Q., Noszticzius, Z. & Swinney, H. L. [1992] "Spatial bistability of two-dimensional Turing patterns in a reaction–diffusion system," *J. Chem. Phys.* **96**, p. 6773

Ouyang, Q., Gunaratne, G. H. & Swinney, H. L. [1993] "Rhombic patterns: Broken hexagonal symmetry," *Chaos* **3**, 707–711.

Ouyang, Q. & Swinney, H. L. [1995] "Onset and beyond Turing pattern formation," in *Chemical Waves and Patterns*, eds. Kapral, R. & Showalter, K. (Kluwer, Dordrecht), pp. 269–295.

Pampaloni, E., Residori, S., Soria, S. & Arecchi, F. T. [1997] "Phase locking in nonlinear optical patterns," *Phys. Rev. Lett.* **78**, 1042–1045.

Pearson, J. E. & Bruno, W. J. [1992] "Pattern formation in an N + Q component reaction–diffusion system," *Chaos* **2**, 513–524.

Pearson, J. E. [1993] "Complex patterns in a simple system," *Science* **261**, 189–192.

Perraud, J.-J., De Wit, A., Dulos, E., De Kepper, P., Dewel, G. & Borckmans, P. [1993] "One-dimensional spirals: Novel asynchronous chemical wave sources," *Phys. Rev. Lett.* **71**, 1272–1275.

Petrov, V., Ouyang, Q. & Swinney, H. L. [1997] "Resonant pattern formation in a chemical system," *Nature* **388**, 655–657.

Pismen, L. M. [1979] "Multiscale propagation phenomena in reaction–diffusion systems," *J. Chem. Phys.* **71**, 462–473.

Pismen, L. M. [1980] "Pattern selection at the bifurcation point," *J. Chem. Phys.* **72**, 1900–1907.

Pismen, L. M. [1994] "Long-scale deformations of resonant 3-dimensional patterns and the structure of confined dislocation," *Phys. Rev.* **E50**, 4896–4900.

Radehaus, C., Willebrand, H., Dohmen, R., Niedernostheide, F.-J., Bengel, G. & Pürwins, H.-G. [1992] "Spatially periodic patterns in a dc gas-discharge system," *Phys. Rev.* **A45**, 2546–2557.

Roberts, A. J. [1985] "An introduction to the technique of reconstitution," *SIAM J. Math. Anal.* **16**, 1243–1257.

Rovinsky, A. B. & Menzinger, M. [1992] "Chemical instability induced by a differential flow," *Phys. Rev. Lett.* **69**, 1193–1196.

Rovinsky, A. B. & Menzinger, M. [1993] "Self-organization induced by the differential flow of activator and inhibitor," *Phys. Rev. Lett.* **70**, 778–781.

Rudovics, B., Dulos, E. & De Kepper, P. [1996] "Standard and nonstandard Turing patterns and waves in the CIMA reaction," *Phys. Scrip.* **T67**, 43–50.

Rudovics, B., Barillot, E., Davies, P. W., Dulos, E., Boissonade, J. & De Kepper, P. [1999] "Experimental studies and quantitative modeling of Turing patterns

in the chlorine dioxide, iodine, malonic acid reaction," *J. Phys. Chem.* **103**, 1790–1800.

Sanz-Anchelergues, A., Zhabotinsky, A. M., Epstein, I. R. & Munuzuri, A. P. [2001] "Turing pattern formation induced by spatially correlated noise," *Phys. Rev.* **E63**, 056124 (1–5).

Schöll, E. [1987] *Nonequilibrium Phase Transitions in Semiconductors* (Springer-Verlag, Berlin).

Scott, S. K. & Showalter, K. [1992] "Simple and complex propagating reaction–diffusion fronts," *J. Phys. Chem.* **96**, 8702–8711.

Setayeshgar, S. & Cross, M. [1998] "Turing instability in a boundary-fed system," *Phys. Rev.* **E58**, 4485–4500.

Setayeshgar, S. & Cross, M. [1999] "Numerical bifurcation diagram for the two-dimensional boundary-fed chlorine dioxide-iodine-malonic acid system," *Phys. Rev.* **E59**, 4258–4264.

Steinbock, O., Kasper, E. & Müller, S. C. [1998] "Complex pattern formation in the polyacrylamide–methylene blue oxygen reaction," *J. Phys. Chem.* **103**, 3442–3446.

Tlidi, M., Dewel, G. & Borckmans, P., unpublished results.

Tóth, A., Lagzi, I. & Horváth [1996] "Pattern formation in reaction–diffusion systems: Cellular acidity fronts," *J. Phys. Chem.* **100**, 14837–14839.

Turing, A. [1952] "The chemical basis of morphogenesis," *Phil. Trans. R. Soc.* **B237**, 37–72.

Tyson, J. J. & Keener, J. P. [1988] "Singular perturbation theory of traveling waves in excitable media (a review)," *Physica* **D32**, 327–361.

Vanag, V. & Epstein, I. R. [2001] "Pattern formation in a tunable medium: The Belousov–Zhabotinky reaction in an aerosol OT microemulsion," *Phys. Rev. Lett.* **87**, 228301.

Vastano, J. A., Pearson, J. E., Horsthemke, W. & Swinney, H. L. [1987] "Chemical pattern formation with equal diffusion coefficients," *Phys. Lett.* **A124**, 320–324.

Vastano, J. A., Pearson, J. E., Horsthemke, W. & Swinney, H. L. [1988] "Turing patterns in an open reactor," *J. Chem. Phys.* **10**, 6175–6181.

Velarde, M. [1981] "Dissipative structures and oscillations in reaction–diffusion systems with and without time delay," *Lecture Notes in Physics* **164**, 248–278.

Verdasca, J., De Wit, A., Dewel, G. & Borckmans, P. [1992] "Reentrant hexagonal Turing structures," *Phys. Lett.* **A168**, 194–198.

Vincent, S. & Perrimon, N. [2001] "Fishing for morphogens," *Nature* **411**, 533–536.

Walgraef, D., Dewel, G. & Borckmans, P. [1980] "Fluctuations near nonequilibrium phase transitions to nonuniform states," *Phys. Rev.* **A21**, 397–404.

Walgraef, D., Dewel, G. & Borckmans, P. [1982] "Nonequilibrium phase transitions and chemical instabilities," *Adv. Chem. Phys.* **49**, 311–355.

Walgraef, D. [1996] *Spatiotemporal Pattern Formation* (Springer-Verlag).

Watzl, M. & Münster, A. F. [1995] "Turing-like spatial patterns in a polyacrylamide-methylene blue-sulfide-oxygen system," *Chem. Phys. Lett.* **242**, 273–278.

Willebrand, H., Niedernostheide, F. J., Dohmen, R. & Pürwins, H. G. [1992] "Stationary and dynamic patterns of current density in gas-discharge systems," in *Oscillations and Morphogenesis*, ed. Rensing, L. (Dekker, NY), pp. 81–109.

Zykov, V. S. [1987] "Simulation and wave processes in excitable media," in *Nonlinear Science Theory and Application* (Manchester University Press).